AD_____
(Leave blank)

Award Number: **W81XWH-09-1-0206**

TITLE: ANTIBODY-FUNCTIONALIZED CARBON NANOTUBE TRANSISTORS AS BIOSENSORS FOR THE DETECTION OF PROSTATE CANCER

PRINCIPAL INVESTIGATOR: Alan Johnson Jr., Ph.D.

CONTRACTING ORGANIZATION: University of Pennsylvania,
Philadelphia PA 19104

REPORT DATE: September 2013

TYPE OF REPORT: Final

PREPARED FOR: U.S. Army Medical Research and Materiel Command
Fort Detrick, Maryland 21702-5012

DISTRIBUTION STATEMENT:

Approved for public release; distribution unlimited

REPORT DOCUMENTATION PAGE

Form Approved
OMB No. 0704-0188

1. REPORT DATE *(DD-MM-YYYY)*	**2. REPORT TYPE**	**3. DATES COVERED** *(From - To)*
September 2013	Final	1 July 2009 - 30 June 2013

4. TITLE AND SUBTITLE
ANTIBODY-FUNCTIONALIZED CARBON NANOTUBE TRANSISTORS AS BIOSENSORS FOR THE DETECTION OF PROSTATE CANCER

5a. CONTRACT NUMBER
W81XWH-09-1-0206

5b. GRANT NUMBER
W81XWH-09-1-0206

5c. PROGRAM ELEMENT NUMBER

6. AUTHOR(S)
Alan Johnson Jr, Ph.D.
Matthew Robinson, Ph.D.
cjohnson@physics.upenn.edu

5d. PROJECT NUMBER

5e. TASK NUMBER

5f. WORK UNIT NUMBER

7. PERFORMING ORGANIZATION NAME(S) AND ADDRESS(ES) =
University of Pennsylvania
3451 Walnut St.
Philadelphia PA 19104-6205

8. PERFORMING ORGANIZATION REPORT NUMBER

9. SPONSORING / MONITORING AGENCY NAME(S) AND ADDRESS(ES)
U.S. Army Medical Research and Materiel Command
Fort Detrick MD 21702-5012

10. SPONSOR/MONITOR'S ACRONYM(S)

11. SPONSOR/MONITOR'S REPORT NUMBER(S)

12. DISTRIBUTION / AVAILABILITY STATEMENT
Approved for public release; distribution unlimited

13. SUPPLEMENTARY NOTES

14. ABSTRACT
Prostate cancer (CaP) is the most commonly diagnosed cancer and second leading cause of cancer deaths among American men and as such represents a major public health issue. CaP displays a range of clinical behaviors, from indolent to aggressive, with development of overt metastatic disease being arguably one of most significant events in the progression of prostate cancer. At present digital rectal exams (DRE) and PSA screening are the "gold-standard" for detection of prostate cancer. In stark contrast to outcomes seen when diagnosed at advanced stages, detection of early-stage, localized, disease often results in successful treatment, with long-term disease-free survival in 60-90% of patients. The work associated with a this grant proposal is focused on the development of a novel biosensor platform, using validated CaP biomarkers as proof-of-concept, that we hypothesize will have increased sensitivity over currently available technologies. Such a device has the potential to improve detection, leading to better patient outcomes.

15. SUBJECT TERMS
Biosensor, Single-wall carbon nanotube, Field Effect Transistor, Osteopontin, OPN, Prostate Specific Antigen, PSA, uPAR, antibody, single-chain Fv, scFv, oriented coupling

16. SECURITY CLASSIFICATION OF:			**17. LIMITATION OF ABSTRACT**	**18. NUMBER OF PAGES**	**19a. NAME OF RESPONSIBLE PERSON**
a. REPORT	**b. ABSTRACT**	**c. THIS PAGE**			USAMRMC
U	U	U	UU	44	**19b. TELEPHONE NUMBER** *(include area code)*

Table of Contents

Final Report for Contract W81XWH-09-1-0206

ANTIBODY-FUNCTIONALIZED CARBON NANOTUBE TRANSISTORS AS BIOSENSORS FOR THE DETECTION OF PROSTATE CANCER

PI – A.T. Charlie Johnson, Jr.

PCRP SYNERGISTIC IDEA DEVELOPMENT AWARD, JOINT PROPOSAL WITH PROPOSAL LOG NUMBER PC080542, FOX CHASE CANCER CENTER, DR. MATTHEW ROBINSON. THE LINKED GRANT AWARD IS W81XWH-09-1-0205.

Introduction

Early detection and differential diagnosis are critical components for the successful treatment of prostate cancer (CaP). The research being carried out under this Synergistic IDEA Award was focused on the development of a novel biosensor platform for the detection of CaP biomakers in biologic fluids, such as serum. The proposed biosensors are comprised of antibody-functionalized single-wall carbon nanotube (swCN) transducers. We demonstrated that the specificity inherent in antibody-antigen interactions, when combined with the swCN platform, could be used to create a novel biosensor platform with increased sensitivity over currently available technologies. The goals for project encompassed the generation of swCN and single-chain antibody (scFv) reagents necessary to carry-out initial proof-of-principle experiments, testing first generation biosensors using simulated serum samples and optimizing the biosensors, and performing a retrospective analysis of patient samples to determine the sensitivity and specificity of the biosensors.

Body

Year 1 of the project was used to develop the methodologies needed for fabrication of the biosensors envisioned in the proposal. Different protein attachement chemistries were developed and optimized. Research carried out during the second year of the grant period focused on testing our first generation SWCN biosensors in simulated serum in preparation for moving into patient samples in year 3. We also used this time period to generate antibodies optimized for site-specific conjugation to the biosensors with the goal of improving sensitivity of the biosensors. The third year of the project was used to further optimize the approach. An unexpected outcome was a demonstration of the application of similar methods to detection of the Lyme disease organism.

Aim 1. Construction and initial validation of a single-wall carbon-nanotube biosensor for detecting prostate cancer

In year 1 of the project we successfully developed a flexible strategy for linking antibodies and antibody fragments to carbon nanotube transistors. The new approach (Fig. 1) relied on the use of carboxylated diazonium salts, which spontaneously form covalent bonds to carbon nanotubes at elevated temperature [1]. A mild diazonium treatment is used, since excessive covalent modification of nanotubes destroys the semiconducting properties necessary for efficient signal transduction [1, 2]. The carboxylic acid functionality of the diazonium salt is activated with a standard EDC/sNHS treatment. In subsequent years we developed the approach further. To date, we have demonstrated that the method may be used to controllably link the nanotube transistor to i) any available amine group by direct incubation in a solution of antibodies [3]; ii) the histidine tag of an engineered protein using Ni-nitrilotriacetic acid chemistry [4]; or iii) an available sulfhydryl group (possibly engineered into the protein) through the use of an iodoacetyl linker molecule (to be published). The alternative chemistries ii) and iii) are shown in the schematic of Fig. 2. This flexibility offers the prospect of rational design of biosensors based on this platform technology. Figure 3 includes an Atomic Force Microscope image showing 23C3 anti-OPN scFv antibodies bound to carbon nanotubes through an amide bond along with a histogram analysis.

Experiments in year 2 were focused on validating our first generation biosensors. It was recognized that compounds in serum, such as salts and albumin, can negatively impact biosensor function and were of concern based on studies performed in year 1. To address these issues, SWCNs were functionalized with anti-OPN scFv (23C3) using the diazonium-based chemistry option i) above, resulting in random scFv orientation since coupling could occur through an amide bond to one of several possible residues. The sensitivity and specificity of the first generation biosensors were evaluated under increasingly complex

conditions. We established an upper concentration limit where phosphate buffer saline had no impact on the electronic transport of 23C3-functionalized SWCN devices (Figure 4, Left). This was followed by the addition of the target antigen (osteopontin, OPN) to the PBS buffer. As seen in Fig 4 (Right), addition of OPN to the buffer resulted in a change in the electronic transport of the devices (specifically, an increase in the on-state current) consistent with an antibody/antigen interaction occurring at the surface of the SWCN device. Responses varied with target concentration in a way that was consistent with the Langmuir-Hill adsorption theory (Figure 5). We demonstrated that 23C3-functionalized SWCN can detect OPN in a dose-dependent manner with a detection limit of 1 pg/mL, a factor of 100-1000 less than conventional ELISA. Non-specific absorption of serum proteins such as albumin to the SWCN is a major concern in the development process. To address this, we established that bovine serum albumin (BSA) at levels of 450 ng/mL had no impact on the ability of the 23C3-functionalized SWCN to detect OPN (90 ng/mL) in simulated serum (Fig 6), thereby demonstrating that the biosensor is both sensitive and selective for OPN.

The experiments described above generated an interest in a more fundamental investigation of the transduction mechanisms of nanotube-based molecular sensors. We started with the hypothesis that electrostatic interactions were critical. This led to the design of a set of molecules that would adsorb onto the surface of nanotube transistors and that contained molecular units that took on known charge states (positive, negative or neutral) in the nanoscale water layer that is known to coat the device substrate under ambient conditions. We demonstrated that the measurement results were as expected from the charge of the adsorbed species, and that the data could be explained in a semiquantitative fashion (Fig. 7). These results, which pave the way towards quantitative models of such biosensors, were published in the Journal of the American Chemical Society. We also were intrigued by the possibility of detection of other disease-relevant biomarkers. An undergraduate student conducted a side project investigating the use of these sensors for detection of the Lyme disease organism. The resulting manuscript was published in Biosensors and Bioelectronics. It generated quite a bit of interest in the Lyme community. Johnson was invited to several Lyme meetings including a NIST Lyme Workshop in June 2013.

Aim 2. Optimizing antibodies to enhance biosensor capabilities

Specificity of the biosensors will be dictated by the antibody that is conjugated to the swCN. Intact monoclonal antibodies (mAbs) with appropriate epitopes and binding characteristics making them suitable for detection of PSA, uPAR and OPN biomarkers in serum are described in the literature and co-crystal structures of a subset are publicly available (Figure 8). We took advantage of co-crystal structure data of ATN-615 (anti-uPAR), 23C3 (anti-OPN), and 8G8F5/2ZCL to create scFv versions of each mAb. Single-chain Fv antibodies are ~25kDa proteins comprised of the antigen binding domains of a mAb [variable heavy (Vh) and variable light (Vl) domains] joined through a flexible peptide linker. Using the publicly available protein sequences we synthesized genes encoding scFv versions of each mAb. Genes, codon-optimized for expression in *E. coli*, were synthesized on NcoI/XhoI fragments in the Vh-linker-Vl orientation using the classic (Gly_4Ser) scFv linker and sub-cloned into the pSYN2 bacterial expression vector inframe with the vector encoded 6xHIS tag to facilitate IMAC purification. Each of the scFv were expressed, purified by sequential IMAC and gel filtration chromatography, and the binding activity of purified fractions characterized via surface plasmon resonance (SPR) using a BIAcore1000. Kinetic analyses of the 23C3 (Fig. 9) and ATN-615 (Fig 10) scFv were performed using CM5 chips coated with commercially available antigens. Theoretical Rmax for the two surfaces were 384 (uPAR) and 115 (OPN) RU. ATN-615 binds to uPAR with an affinity of 7.9×10^{-10} M and 23C3

binds to OPN with an affinity of 2.9 x 10^{-10} M. The observed Rmax for both surfaces was consistent with surfaces that were at least 90% active. In contrast to ATN-615 (Figure 11, right panel) and 23C3 (data not shown), which chromatographed over a Hi Prep 16/60 Sephacryl S-100 size exclusion column as a single peak of a size consistent with being 25 kDa, the 8G8F5/2ZCL anti-PSA scFv purified as three distinct peaks ranging in size from 25 kDa and larger (Figure 11, left panel). When analyzed by SDS-PAGE peaks resolved as a single 25 kDa protein (Figure 12A). This data is consistent with the 8G8F5/2ZCL scFv forming higher-order aggregates, a known issue with some scFv. Standard approaches to alter length and temperature of induction failed to improve yields of monomeric scFv (data not shown). The 25kDa 8G8F5/2ZCL monomeric scFv is active for binding to recombinant PSA as judged by SPR (theoretical Rmax = 164, observed Rmax = 64) (Figure 12B). The yields and overall stability of the 8G8F5/2ZCL scFv made it unusable for conjugating to NT-FET devices. Cysteine residues were engineered into the framework to overcome this stability/aggregation issue by facilitating formation of a stabilizing disulphide bond between the Vh and Vl domains of the scFv. Expression of the disulphide-stabilized 8G8F5/2ZCL was carried out in a mammalian expression system (Figure 13). The disulphide-stabilized scFv was expressed at 40-times higher levels than the corresponding non-stabilized parental scFv expressed in E. coli and chromatographed over a gel filtration column mainly as a monomer. This stabilized 8G8F5/2ZCL retained activity as judged by its ability to immunoprecipitate (IP) PSA that was excreted into growth media by LNCaP cell line (Figure 14). Specificity of the IP was controlled for by the use of an anti-HER3 scFv, which failed to IP PSA from the growth media. The disulphide-stabilized 8G8F5/2ZCL represents a potential path forward for use on NT-FETs. However, use of disulphide-stabilized scFv may limit their utility for thiol-directed coupling strategies (Figure 2, see below). In work undertaken in parallel to this project Dr. Robinson is collaborating with a colleague (Roland Dunbrack, Ph.D.) to generate thermally stable scFv through a molecular modeling approach. We believe that the work being carried out under that collaboration will be directly applicable to the 8G8F5/2ZCL scFv moving forward and can be used to generate a thermally stable anti-PSA that does not rely upon disulphide-stabilization.

A goal of the proposed work was to evaluate the impact of site-directed vs random coupling of the antibodies to the NT-FET sensor. Our initial proposal was to use site-directed mutagenesis to incorporate a free cysteine residue into the scFv to facilitate either thiol- or maleimide-based coupling strategies (Figure 2). Free cysteine residues were incorporated into two locations, the C-terminal tail and the linker connecting the Vh and Vl domains, in the ATN-615 and 23C3 scFv. Both locations are predicted to result in scFv coupling in a manner that oriented the antigen-binding site away from the SWCN surface. However, incorporation of the free cysteine residues into the 23C3 and ATN-615 scFv resulted in complications associated with purification and activity. ATN-615 was purified from bacterial expression system at approximately 0.5 mg/L and chromatographed over a size exclusion column as a single peak consistent with its predicted molecular weight of 26kDa. In stark contrast, incorporation of a free cysteine at the C-terminal tail of ATN-615 to create ATN615-cys resulted in lower levels of expression and aggregation of the scFv. Similar results were seen with 23C3 as well (data not shown). The behavior of the 23C3 and ATN-615 scFv is contrasted by the behavior of the 4D5-cys scFv that was created as a control. 4D5 scFv was modified in a manner identical to ATN-615 and 23C3 to incorporate a free cysteine at the C-terminus (hu4D5-cys). Under identical conditions the ATN615-cys, 23C3-cys, and hu4D5-cys proteins were expressed to roughly equal levels (~ 0.5 mg/L) but unlike ATN615-cys and 23C3-cys, hu4D5-cys migrated as a single 26kDa species. Purified hu4D5-cys as it could selectively IP its target antigen (HER2).

Based on our understanding of the detection mechanism, which was further elucidated by the work detailed above, we hypothesized that bringing antigens closer to the sensor surface would improve detection limits (i.e increase sensitivity) of the biosensors. In addition to providing a uniform surface, we proposed that site-directed conjugation would allow us to directly test this hypothesis. Our initial proposal focused on the use of thiol-based coupling of scFv using chemical linkers of varying lengths to increase this distance. Because of issues associated with the production and stability of the cysteine-modified 23C3 and ATN-615 scFv, we were unable to directly test this hypothesis. However, although initially developed as a control antibody the 4D5-cys scFv has the appropriate properties for its use in testing this hypothesis. To facilitate testing we have optimized conditions to generate Fab' fragments of trastuzumab (Figure 15); the hu4D5 scFv was constructed from the trastuzumab amino acid sequence and exhibits identical monovalent binding characteristics to trastuzumab. As depicted in Figure 15 a Fab' (comprised on variable and first constant domains) of trastuzumab, when coupled through its C-terminal cysteine is predicted to double the distance between the NT-FET and antigen binding site as compared to the scFv-cys. We have optimized conditions to generate hu4D5 Fab' (Figure 15) but a direct side-by-side comparison of the sensitivity achievable with the 4D5-cys scFv and Fab' remains to be performed. However, work carried out using commercially available antibodies specific for a Lyme disease biomarker demonstrated a detection limit of 1ng/mL. This detection limit is approximately 1000x higher than what we were able to achieve with scFv antibodies directed against OPN (Figure 5). This data, although not conclusive, is consistent with our original hypothesis and supports the use of scFv antibodies to optimize the sensitivity and specificity of NT-FET biosensors

As stated above, simultaneous to our work here we have developed the ability to conjugate proteins to NT-FET devices through the 6xHIS purification tag that is universally present at the C-termini of our scFv. This provides us with a strategy to couple scFv in an oriented fashion without the need for additional modification steps that we have demonstrate can deleteriously affect the stability or antigen binding capabilities of the scFv. For other purposes we have begun creating a vector that will allow for expression of C-terminally 6xHIS-tagged Fab fragments in *E. coli*. Once engineered, comparing His-tagged Fab and scFv versions of each antibody via the His-tag conjugation strategy will provide an alternative to the proposed chemical conjugation strategies. Although cysteine-based methods can not be ruled out we envision that Ni-NTA coupling will provide a rapid and robust approach for moving the NT-FET biosensors toward clinical testing.

<u>Aim 3. Validation of swCN biosensors in patient samples</u>

Over the course of this grant period we maintained an exempt IRB approval granting us access to serum/plasma samples from both CaP and normal volunteers housed in the Fox Chase Cancer Center Biosample Repository. The samples housed in this repository are highly annotated and include > 2,400 plasma/serum and 1,300 tissue samples from CaP patients, as well as similar numbers of samples from normal volunteers. The small volumes and non-renewable nature of these samples make them an extremely valuable resource. Until robust strategies can be developed and validated using simulated serum samples, analysis of clinical samples was seen as unwarranted.

Although highly sensitive detection of CaP biomarkers was observed in synthetic serum with defined levels of albumin; levels of albumin up to 450 μg/L did not impair detector function. This level of albumin is 75 – 110 times lower than the level of albumin found in patient serum. The major hurdle to be overcome is the development of a robust protocol for the removal of serum albumin from patient samples without altering biomarker levels. Strategies must be able to account for the small volumes and the varied behavior of multiple biomarkers if multiplex detection is going to be employed. The issues

with currently available technology are seen in Figure 3.1. Cell growth media containing serum albumin (5 g/L, 10 times less than in patient samples) and IgG (100 μg/mL, $6x10^{-7}$ M, 200x higher on a mass basis than upper concentrations of OPN used in studies outlined above) as a model protein were chromatographed over Sepharose Blue, a commercially resin that binds albumin and is used for removal of albumin from samples. As depicted in the SDS-PAGE analysis of the column fractions, the majority of albumin bound to Sepharose Blue as was expected, and was eluted from the resin by high salt wash. However, despite the low level of starting serum albumin, a significant portion remained in the flow through (i.e. sample for biomarker detection with NT-FET). More problematic was the unanticipated removal of the entire IgG sample (model biomarker) from the NT-FET sample (i.e. flow through) despite the high starting concentration. Methods to overcome these problems must be identified prior to starting a retrospective analysis of patient samples.

Key Research Accomplishments

- Isolated and characterized functional scFv antibodies against each of the three target antigens
    - Targets are osteopontin (OPN), Urokinase Plasminogen Activator Receptor (uPAR) and prostate specific antigen (PSA)
    - Measured binding affinity for two of the three scFv by surface plasmon resonance
        - 23C3 and ATN-615 bind to OPN and uPAR, respectively, with sub-nanomolar affinity
        - Stability of anti-PSA scFv 8G8F5 prevented measurement of binding affinity. See below for approaches to overcome this negative result.
- Developed two site-directed conjugation protocols for coupling scFv to swCN sensors
    - Ni-NTA based conjugation through the 6XHIS purification tag located at C-terminus of scFv
    - Thiol-coupling through cysteine residues that were engineered into the scFv at defined sites
- Demonstrated specificity and detection limits of antibody-functionalized swCN biosensors using OPN as model system.
    - Detection limits and specificity were carried out in both an optimized buffer system and in synthetic serum
    - Identified need for developing a method to robustly remove serum albumin from patient samples without altering biomarker concentration. Work is ongoing to determine how this can best be accomplished without altering concentration of biomarkers of interest
- Further elucidated the mechanism of voltage gating of the CNT FET
    - Using acidic and basic small molecule compounds demonstrated that distance between compounds and sensor surface controlled magnitude of gate voltage shift
    - Demonstrated that biomarker detection with an intact IgG was 1ng/mL. This is 1000x higher than the detection limit when using scFv antibodies, supporting our initial hypothesis that engineering scFv antibodies to bring antibody/antigen interaction closer to the sensor surface would be critical for improving detection limits.
- Demonstrated specificity and detection limit of the antibody-functionalized carbon nanotube biosensor technique for the detection of Lyme disease
- Identified need for enhancing stability of the scFv coupled to the sensor surface. Evaluated two different approaches to enhance stability
    - “Classic approach” of incorporating disulphide bond between Vh and Vl frameworks

        - Incorporated disulphide bond into 8G8F5 anti-PSA.
        - Improved overall stability, resulting is essentially all monomeric scFv, as judged by elution pattern on gel filtration column
        - Improved total yield from 0.15 mg/L to 6 mg/L
        - Stabilized scFv retained ability to bind PSA as measured by immunoprecipitation of native PSA out of LNCaP conditioned medium.
    - "Molecular modeling approach"
        - In silico methods used to predict CDR structure and then identify optimal framework for CDR grafting.
        - Current data demonstrates the validity of using the novel modeling approach to pair CDRs with highly stable frameworks. Work is ongoing with manuscript submission expected in the next 6 months.

Reportable Outcomes

- Final IRB approval was obtained for clinical protocol to obtain CaP samples from the FCCC biosample repository
- This research led directly to a new collaboration between the initiating PI (Dr. Matthew Robinson) and Dr. Gianluca Piazza (University of Pennsylvania, Department of Electrical and Systems Engineering) to develop a second type of sensor platform. Research is focused on detection of immune modulatory molecules related to CaP.
    - Collaboration resulted in two successful applications for external funding from The Nanotechnology Institute (an initiative of the PA Department of Community and Economic Development, funded by the Ben Franklin Technology Development Authority).
    - Additional funding application was also submitted to the National Science Foundation
- Results of studies directly, and indirectly, related to the goals of the grant were published in high impact journals. References are
    - Lerner M, D'Souza JW, Pazina T, Dailey J, Goldsmith B, Robinson MK*, Johnson, AT* Hybrids of a genetically engineered antibody and a carbon nanotube transistor for detection of prostate cancer biomarkers. *ACS nano* 6(6):5143-5149, 2012. PMCID: PMC3383883 * = co-corresponding authors (5-Year Impact Factor: 12.52).
    - Goldsmith BR, Mitala JJ, Josue J, Castro A, Lerner MB, Bayburt TH, Khamis SM, Jones RA, Brand JG, Sligar SG, Luetje CW, Gelperin A, Rhodes PA, Discher BM, Johnson AT. Biomimetic chemical sensors using nanoelectronic readout of olfactory receptor proteins. ACS nano 5(7):5408-5416, 2011 PMID:21696137. (5-Year Impact Factor: 12.52)
    - Lerner MB, Dailey J, Goldsmith BR, Brisson D, Johnson AT. Detecting Lyme disease using antibody-functionalized single-walled carbon nanotube transistors. *Biosensors and Bioelectronics* 45:163-167, 2013 (5-Year Impact Factor: 5.39)
    - Lerner MB, Resczenski JM, Amin A, Johnson RR, Goldsmith JI, Johnson AT. Toward quantifying the electrostatic transduction mechanism in carbon nanotube molecular sensors. *J Am Chem Soc* 134(35):14318-14321 (5-Year Impact Factor: 10.24)
- Site-directed conjugation of scFv to swCN surface was included in invited oral presentations at multiple international conferences: Center for Integrated NanoTechnologies (CINT) User Meeting, Albuquerque, New Mexico, August 2010; Nanotube 2010 (NT10) meeting, Montreal, Canada (June 2010), Gordon Research Conference on Physics Research and Education, South

Hadley, Massachusetts, June 2010; "Nano Helps Bio" Conference, Santa Fe, New Mexico, April 2010.

- Research results were presented in poster format at 15th Annual and 16TH Annual Postdoctoral and Graduate Student Research Symposium, FCCC.
- Research results were presented at the IMPaCT conference in two posters given by Drs. Johnson and Robinson, Orlando, FL (March 2011).
- Research results were presented in poster format at the American Physical Society Meeting, Dallas, TX (March 2011)
- Research results were presented in an Invited lecture at the Annual Meeting of the Chemical Physical Society. Guangzhou, China. September 2012.
- Research results were presented at the 10TH Prestige Workshop of the Korean Academy of Science and Technology. Seoul, South Korea. May 2012.
- Research results were presented at GE Global Research Laboratory. Niskayuna, New York. November 2012.
- Research results were presented to the Prostate Cancer Advocacy Group, Man to Man. Bryn Mawr Hospital Health Center, Newtown Square, Pennsylvania. January 2013.
- Research results were presented at the 2013 Bioeleectronics and Biosensing Symposium, NanoSafe Center. West Virginia University, Morgantown, West Virginia. April 2013.
- Research results were presented as an invited lecture at Measurement – The Foundation for the Effective Diagnosis and Measurement of Lyme Disease. Gaithursburg, Maryland. June 2013.
- Research results were presented as an invited lecture at the Telluride Workshop on the Chemistry and Physics of Defects in Carbon Nanotubes. Telluride Colorado. July 2013
- Research results were presented as an Invited lecture at the 2013 Meeting of the American Chemical Society, Indianapolis, Indiana. September 2013
- Research results were presented at an Invited lecture at the Food and Drug Administration, Bethesda, Maryland. September 2013

Conclusions

As a direct result of close interactions between the Johnson and Robinson groups over the course of this synergistic IDEA award we have been able to successfully test the underlying hypothesis of this work, that antibody-functionalized NT-FET-based biosensors can be used for the detection of serum-based biomarkers. The results of those studies were published in a high-impact journal that ranks near the top in its field. During the time frame of this grant we identified a number of hurdles, not envisioned at the time of the initial proposal, which needed to be addressed in order to optimize the biosensor platform. Work carried out to address those hurdles has also been published in a series of papers. The major obstacle outlined in the original proposal that remains unsolved is the ability to detect biomarkers in patient serum. Highly sensitive detection was observed in simulated serum with reduced levels of albumin strategies but development of effective procedures to reduce albumin, and other proteins, in patient samples without altering biomarker levels remains as a stumbling block. Work will continue through additional funding mechanisms to overcome this hurdle.

References

1. J. L. Bahr, J. P. Yang, D. V. Kosynkin, M. J. Bronikowski, R. E. Smalley and J. M. Tour, J. Am. Chem. Soc. **123** (27), 6536-6542 (2001).
2. R. A. Graff, T. M. Swanson and M. S. Strano, Chem Mater **20** (5), 1824-1829 (2008).
3. M. B. Lerner, J. D'Souza, T. Pazina, J. Dailey, B. R. Goldsmith, M. K. Robinson and A. T. C. Johnson, ACS Nano **6**, 5143-5149 (2012).
4. B. R. Goldsmith, J. J. Mitala, J. Josue, A. Castro, M. B. Lerner, T. H. Bayburt, S. M. Khamis, R. A. Jones, J. G. Brand, S. G. Sligar, C. W. Luetje, A. Gelperin, P. A. Rhodes, B. M. Discher and A. T. C. Johnson, ACS Nano **5** (7), 5408-5416 (2011).

Appendices and Supporting Data

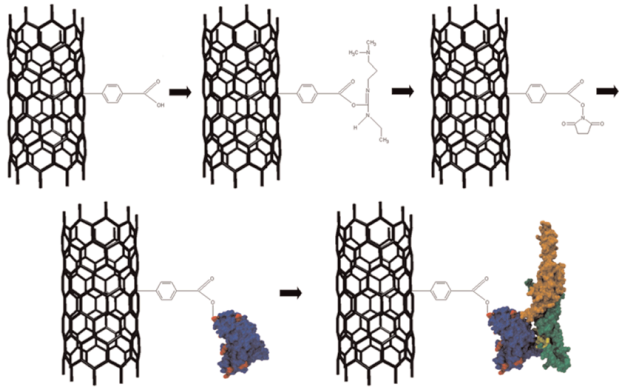

Figure 1 Schematic of the attachment chemistry developed for the project. First, a defect is created on the nanotube sidewall using a carboxylated diazonium salt. The defect is then activated by EDC and stabilized with NHS. ScFv protein displaces the NHS, with random orientation. OPN binds preferentially to the scFv in the detection step.

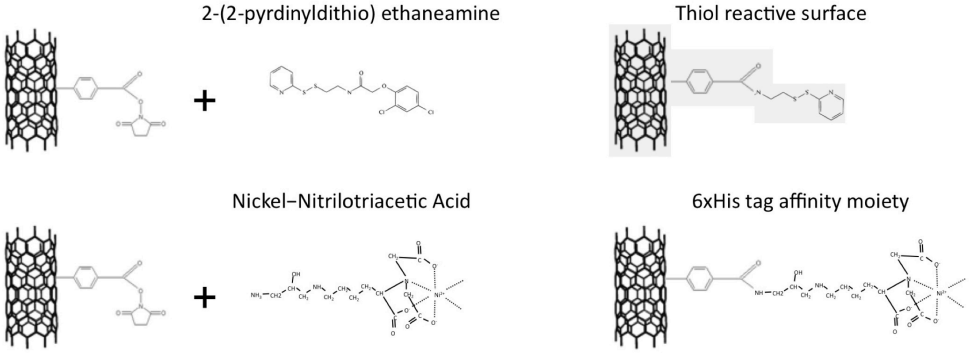

Figure 2. Strategies for activating the nanotube sidewall to promote site-specific conjugation through either cysteines (thio-reactive) or a histidine tag.

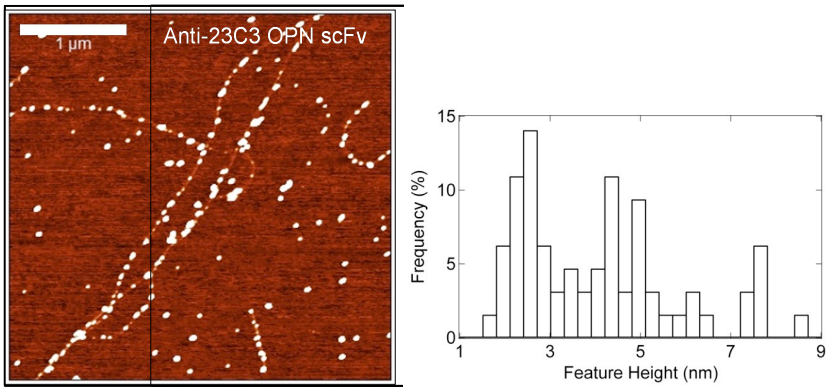

Figure 3. Left: Atomic Force Microscope image of carbon nanotubes chemically functionalized with 23C3 anti-OPN scFv antibodies. White dots in the image are assumed to be the scFv. White dots that form a line-like structure are known to be anchored to a carbon nanotube. Isolated white dots are presumed to be non-specifically bound on the substrate. Lateral range 2.5 µm, height scale, 10 nm. **Right:** Histogram of the heights of the white features bound to the nanotube in Fig 2a shows a maximum at ~ 2.5 nm, consistent with the expected height of scFv antibodies. Secondary maxima at 5 nm and 7.5 nm are attributed to small aggregates of scFv antibodies. The total number of features analyzed is 180.

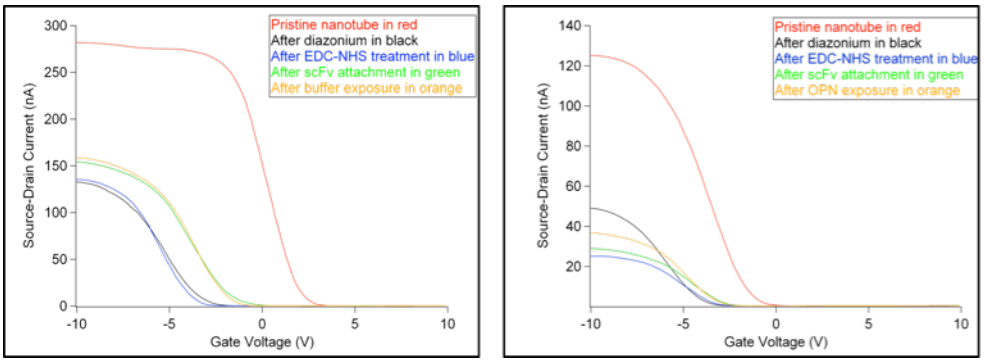

Figure 4. Left: Buffer containing less than 10mM salt does appreciably change the transport properties of the antibody-functionalized SWCN. **Right:** OPN exposure results in an increase in source drain current consistent with interaction between 23C3 scFv and antigen target.

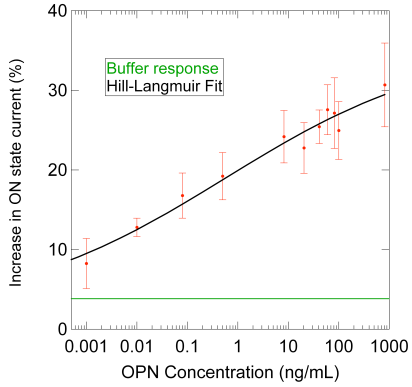

Figure 5. Response versus concentration data show excellent agreement with the prediction of Hill-Langmuir adsorption theory. From this data, the scFv affinity is approximately 500 pg/mL, and the detection limit is 1 pg/mL

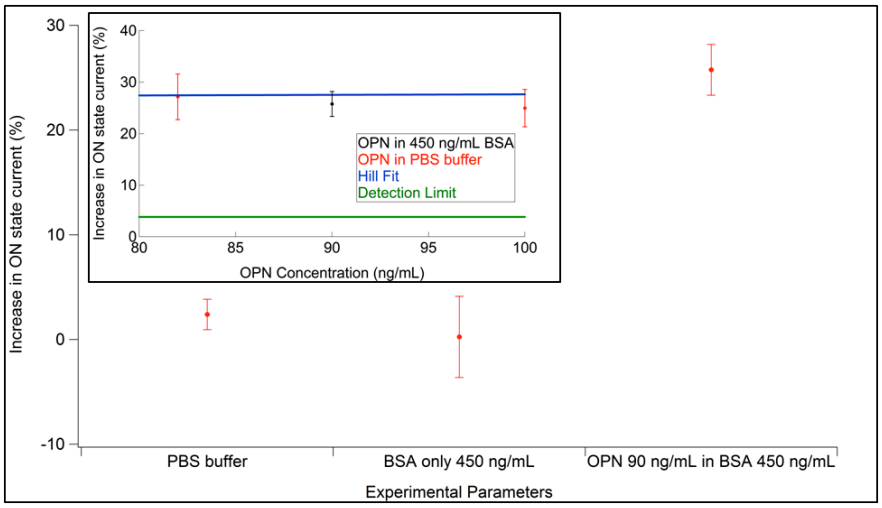

Figure 6. Control data for the functionalized SWCN FET. Response to unspiked, diluted PBS buffer is shown in green. Response to diluted PBS spiked with bovine serum albumin (BSA) at 450 ng/mL is indistinguishable from response to unspiked PBS. Inset: 90 ng/mL OPN in BSA background produces a response equal to that found for OPN in plain buffer.

.

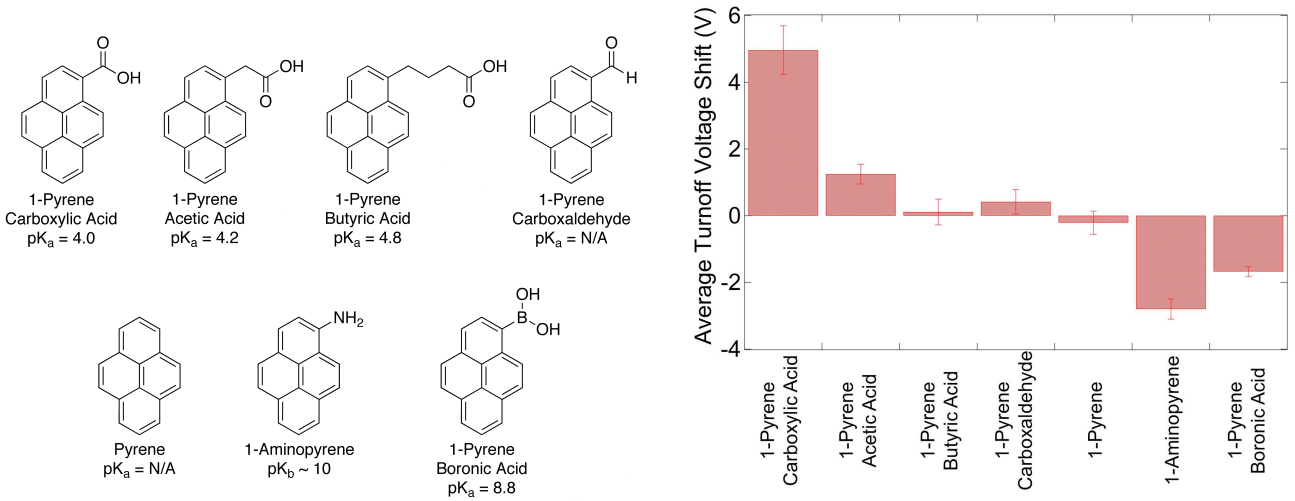

Figure 7. Left: Pyrene compounds utilized to test the importance of the electrostatic interaction for the response mechanism of nanotube biosensors. The pyrene moiety causes these molecules to bind to the nanotube sidewall. The remaining chemical component leads to a known charge (negative, neutral, or positive) at a known location to develop in the nanoscale water layer bound to the surface. **Right:** Average threshold voltage shift caused by exposure to pyrene compounds. The trend observed is consistent with the expected sign and location of the charge induced in the adsorbed pyrene species. Each value is the average of results from 15-20 devices; error bars are the standard errors of the mean.

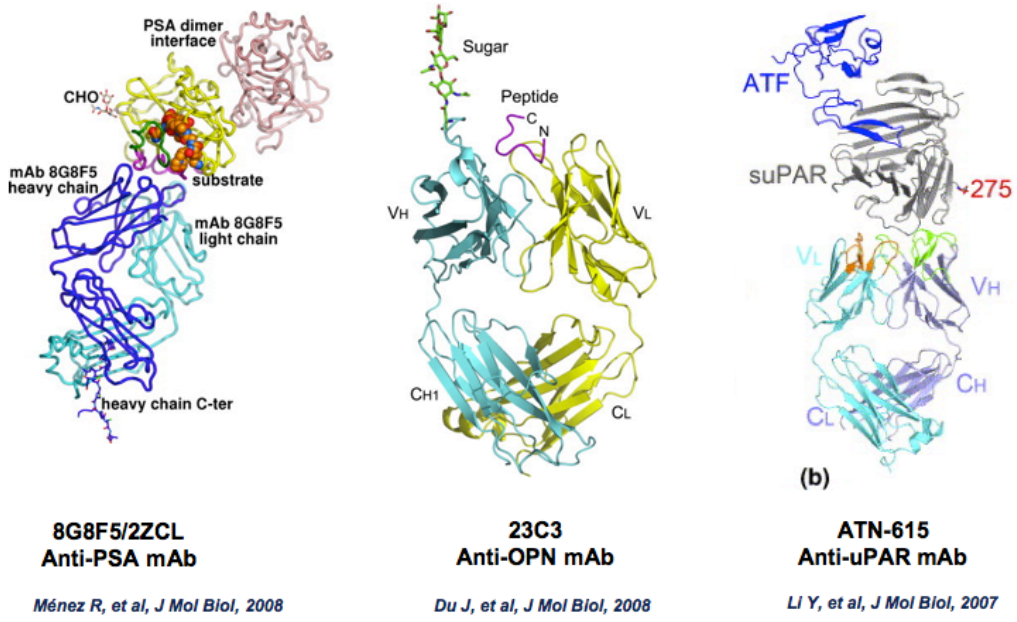

Figure 8. Co-crystal structures of relevant antibody Fab fragments bound to biomarkers of interest. Monoclonal antibodies specific for biomarkers of interest were identified in the literature. Co-crystal structures depicted above demonstrate that the mAb bind appropriate epitopes to be used for detection of the antigens in serum.

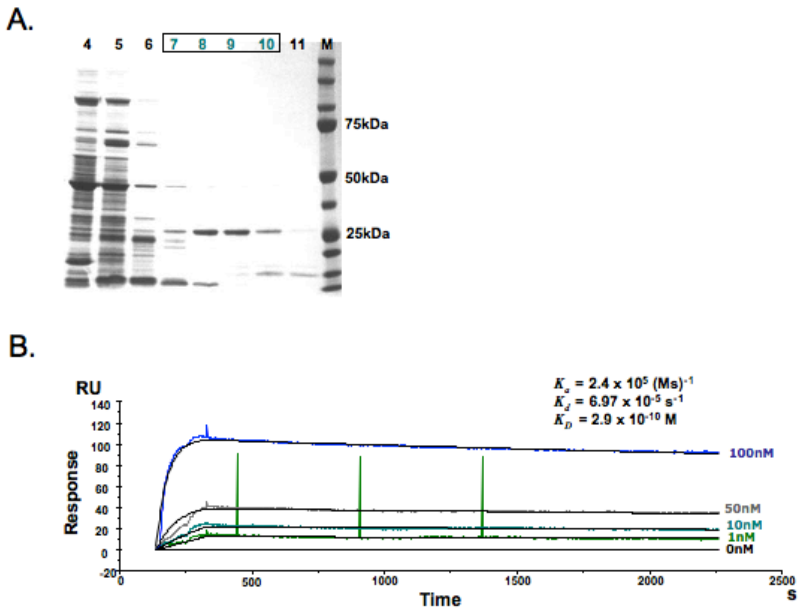

Figure 9. Characterization of the anti-OPN 23C3 scFv
A) SDS-PAGE analysis of IMAC purification over Ni-NTA column. Fractions 7 – 10 were pooled, subjected to gel filtration chromatography. B) Gel filtration fractions containing purified scFv were analyzed by SPR and kinetic constants determined with BIAevaluation using a 1:1 binding model and global fit analysis.

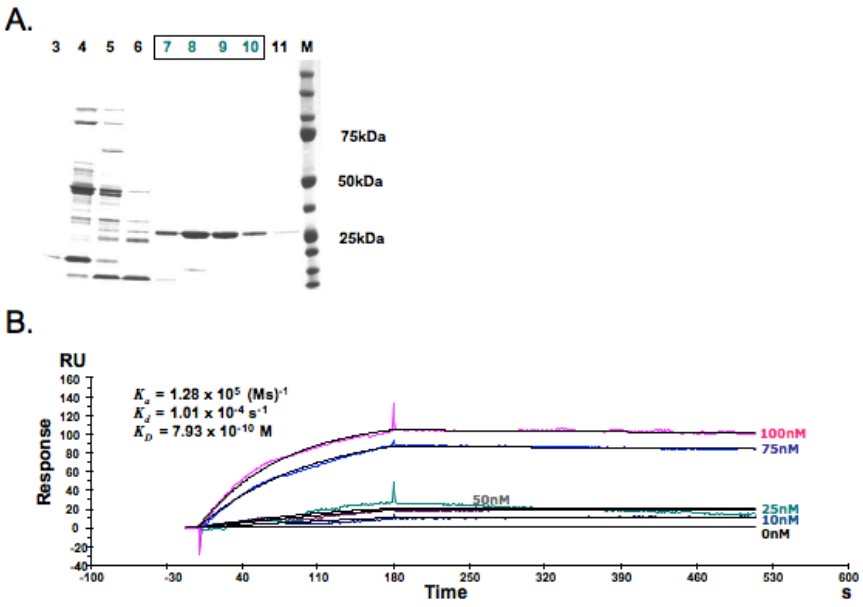

Figure 10. Characterization of the anti-uPAR ATN-615 scFv
A) SDS-PAGE analysis of IMAC purification over Ni-NTA column. Fractions 7 – 10 were pooled, subjected to gel filtration chromatography. B) Gel filtration fractions containing purified scFv were analyzed by SPR and kinetic constants determined with BIAevaluation using a 1:1 binding model and global fit analysis.

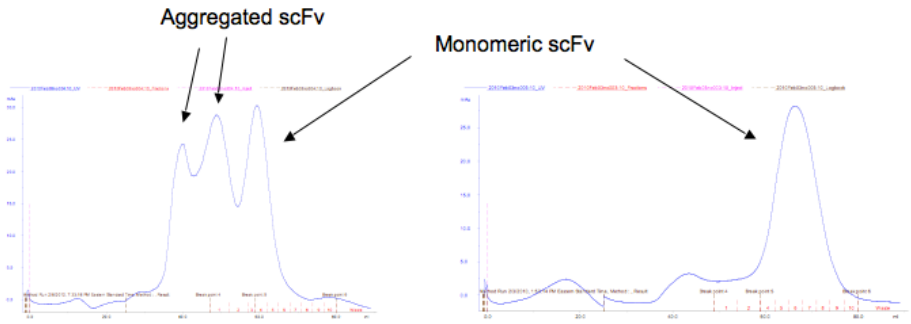

Figure 11. Gel filtration analysis of 8G8F5/2ZCL and ATN-615 scFv
The 8G89F5/2ZCL (left panel) resolved as three distinct peaks as compared to the single peak seen with theATN-615 scFv (right panel).

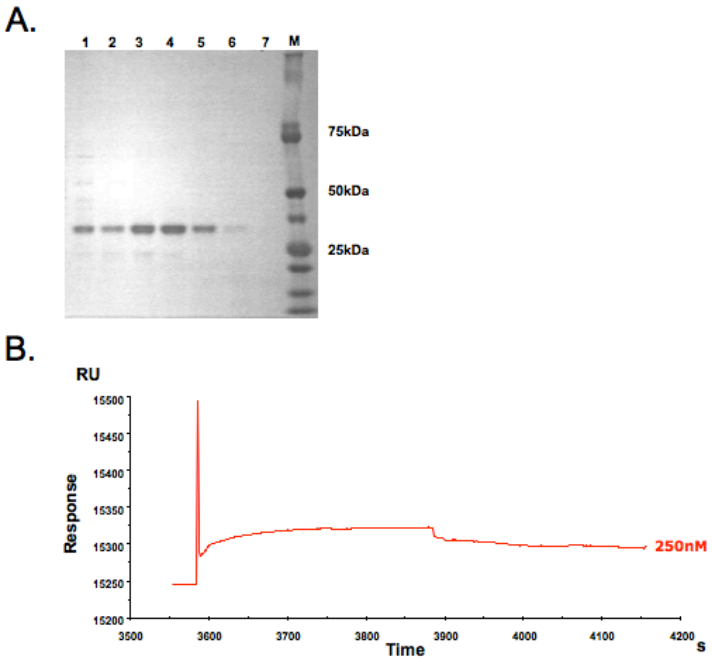

Figure 12. 8G8F5/2ZCL scFv
A) SDS-polyacrylamide gel electrophoresis analysis of S-100 gel filtration fractions across all three peaks, suggesting that high molecular weight peaks are aggregated forms of the scFv. B) Monomeric 8G8F5/2ZCL binds to recombinant PSA (R&D) as analyzed by SPR

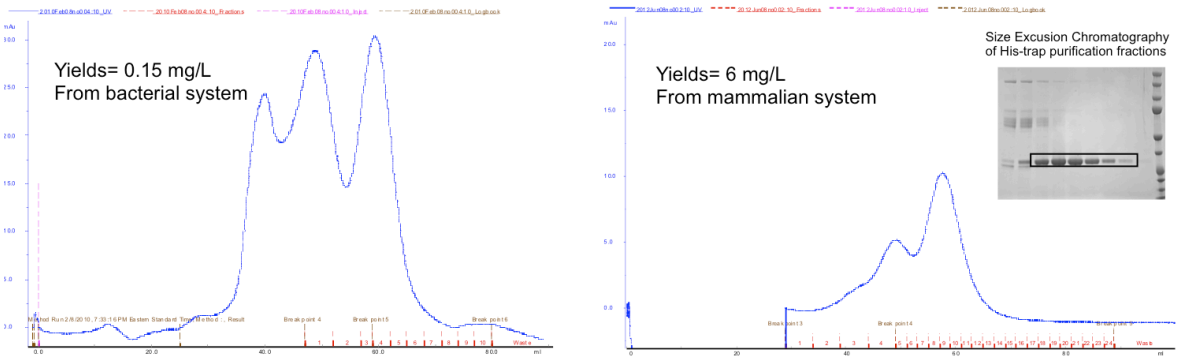

Figure 13. Stability engineering of anti-PSA scFv

Left panel: As seen in Figure 2.5 gel filtration chromatograph of 8G8F5 scFv purified from bacterial expression system shows higher order multimers consistent with inherent instability of scFv. Yields were 0.15mg/L of culture.

Right panel: gel filtration chromatograph of 8G8F5:S=S scFv. Yield were increased to 6 mg/L and majority of scFv migrated as monomer. Shoulder peak corresponds to albumin observed in SDS-PAGE analysis.

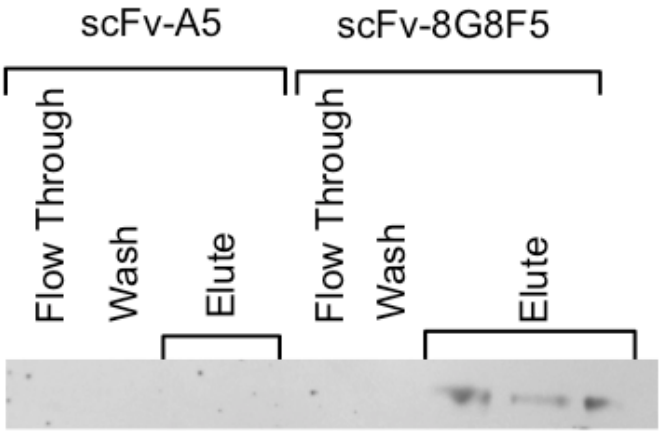

Figure 14. 8G8F5:S=S retains ability to bind PSA

Disulphide stabilized 8G8F5 immobilized on Ni-NTA beads through its 6XHIS affinity tag was capable of immunoprecipitating PSA from LNCaP conditioned medium as judged by Western blot analysis. The control anti-HER3 A5 scFv failed to IP PSA, demonstrating the specificity of 8G8F5.

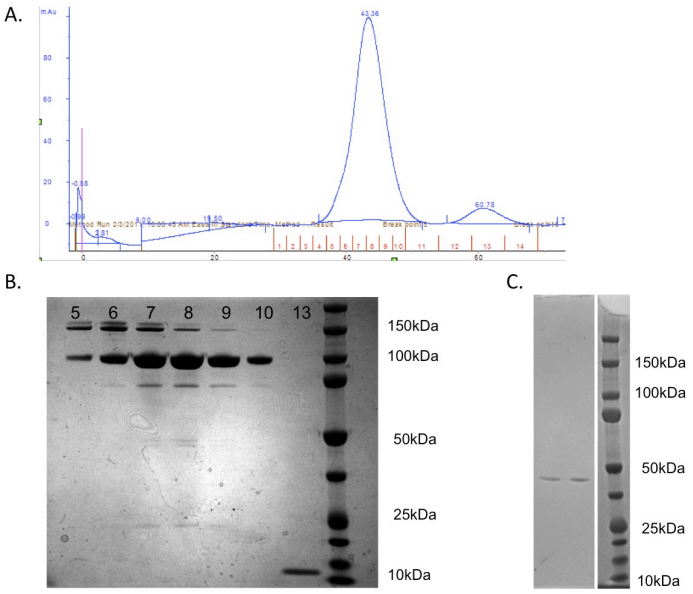

Figure 15. Generation of hu4D5 Fab' for testing the impact of distance on biosensor function.
A) Chromatograph of Fab'$_2$ after pepsin digestion of hu4D5. B) SDS-PAGE analysis of column fractions from "A". C) Native PAGE after reducing fraction 10 to Fab'

Hybrids of a Genetically Engineered Antibody and a Carbon Nanotube Transistor for Detection of Prostate Cancer Biomarkers

Mitchell B. Lerner,[†] Jimson D'Souza,[‡] Tatiana Pazina,[‡] Jennifer Dailey,[†] Brett R. Goldsmith,[†] Matthew K. Robinson,[‡,*] and A. T. Charlie Johnson[†,*]

[†]Department of Physics and Astronomy, University of Pennsylvania, 209 S. 33rd Street, Philadelphia, Pennsylvania 19104, United States and
[‡]Developmental Therapeutics Program, Fox Chase Cancer Center, 333 Cottman Avenue, Philadelphia, Pennsylvania 19111, United States

ABSTRACT

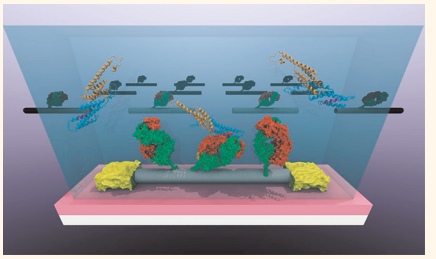

We developed a novel detection method for osteopontin (OPN), a new biomarker for prostate cancer, by attaching a genetically engineered single-chain variable fragment (scFv) protein with high binding affinity for OPN to a carbon nanotube field-effect transistor (NT-FET). Chemical functionalization using diazonium salts is used to covalently attach scFv to NT-FETs, as confirmed by atomic force microscopy, while preserving the activity of the biological binding site for OPN. Electron transport measurements indicate that functionalized NT-FET may be used to detect the binding of OPN to the complementary scFv protein. A concentration-dependent increase in the source—drain current is observed in the regime of clinical significance, with a detection limit of approximately 30 fM. The scFv-NT hybrid devices exhibit selectivity for OPN over other control proteins. These devices respond to the presence of OPN in a background of concentrated bovine serum albumin, without loss of signal. On the basis of these observations, the detection mechanism is attributed to changes in scattering at scFv protein-occupied defect sites on the carbon nanotube sidewall. The functionalization procedure described here is expected to be generalizable to any antibody containing an accessible amine group and to result in biosensors appropriate for detection of corresponding complementary proteins at fM concentrations.

KEYWORDS: biosensor · carbon nanotube · field effect transistor · cancer diagnostics

Prostate cancer (CaP) is a major public health issue as the most commonly diagnosed cancer and second leading cause of cancer deaths among American men.[1] Detection of early stage cancer often results in successful treatment, with long-term disease-free survival in 60—90% of patients. One methodology for early disease detection is biomarker sensing and quantification through use of specialized assays. Biomarkers of cancer are molecular or tissue-based signatures of disease that provide either diagnostic or prognostic insight into disease etiology and/or progression. In the case of CaP, levels of prostate specific antigen (PSA) in patient serum above 4 ng/mL[2] have traditionally been used as a predictive biomarker of disease. However, PSA tests are prone to both false positives and false negatives, causing healthy men to undergo unnecessary medical procedures as well as men with cancer to go undiagnosed.[3] This has resulted in the utility of PSA as a broad-based screening tool being called into question and supports the need for identification of additional biomarkers of CaP. One potential new biomarker of CaP is osteopontin (OPN).[4] OPN is a proinflammatory cytokine that regulates bone homeostasis through its effects on osteoclast function.[5] OPN is being investigated both as a therapeutic target and as a biomarker for diseases such as arthritis and cancer.[6,7] Progression of CaP, as well as other cancers, is often associated with metastasis to bone. OPN is thought to play a role in the metastatic process and development of metastatic disease correlates with increased serum levels of OPN.[8] Monoclonal antibodies (mAbs) specific for OPN, such as the 23C3 mAb, represent promising therapeutic and diagnostic agents.[9,10] Traditional protein detection methods such as ELISA are quite sensitive, but have proven problematic for quantification of OPN.[11] They also require pure samples, lengthy processing times, and expertise in molecular biology and could be expensive.[12] As a result, cost-efficient, easy to implement immunosensors with comparable

* Address correspondence to matthew.robinson@fccc.edu; cjohnson@physics.upenn.edu.

Received for review February 23, 2012 and accepted May 10, 2012.

Published online 10.1021/nn300819s

or better sensitivity than an ELISA assay would be highly desirable. Recently, it was reported that biosensors based on semiconducting nanowire field effect transistors (FETs) achieved detection limits for PSA of 5 pM for time domain measurements and 150 fM for frequency domain measurements that require more complex electronic instrumentation.[13] This motivated us to explore whether further sensitivity enhancements could be achieved through the use of carbon nanotube FETs tightly coupled to engineered antibody elements.

Carbon nanotube field effect transistors (NT-FETs) provide a unique transduction platform for chemical and biomolecular detection.[14−16] Tailored and specific detection may be accomplished by chemically functionalizing the NT-FET with a selected antibody to create a hybrid nanostructure. Proteins that bind to the hybrid alter the electrical properties of the NT-FET *via* several mechanisms,[17] allowing direct detection as a change in the transistor conduction properties such as threshold voltage or ON state current. Ease of fabrication, well-understood carbon surface chemistry, and fast electronic readout make NT-FET-based hybrids desirable as sensors either in an antibody−antigen detection scheme or as a vapor sensor suitable for more complex system architectures characteristic of mammalian olfaction.[18−21] Large arrays of such devices could potentially assist medical diagnosis through simultaneous measurement of hundreds of biomarkers using a single small-volume sample.[22−24]

The binding specificity inherent in mAbs makes them promising agents for use as both targeted therapies and as reagents for detecting biomarkers of disease. The murine mAb 23C3 recognizes a conserved, linear peptide (^{43}WLNPDP^{48}) within OPN. When administered to animals, the 23C3 immunoglobulin (IgG) induced a therapeutic response in a collagen-induced model of arthritis[6] and led to its humanization (Hu23C3) through a CDR-grafting approach in preparation for transition into clinical trial.[25] Effective use of targeted therapies for the treatment of cancer and other diseases requires paired diagnostic tests to detect the presence or absence of relevant biomarkers.

In this study we have engineered the 23C3 mAb into a single-chain variable fragment (scFv) antibody.[26] ScFv antibodies are composed of the variable heavy and variable light domains of the parental IgG, fused by a short peptide linker, and retain the antigen-binding properties of the intact IgG. The 23C3 mAb was converted to an scFv in an effort to optimize its structure for use on NT-FET-based biosensors for the detection of OPN in bodily fluids. Here we found that the 23C3 scFv retains its ability to bind OPN, which should allow it to be an effective diagnostic surrogate for the Hu23C3 therapeutic antibody. In addition, its small size compared to the parental IgG (25 and 150 kDa, respectively) is hypothesized to provide advantages over the parental IgG when used for production of

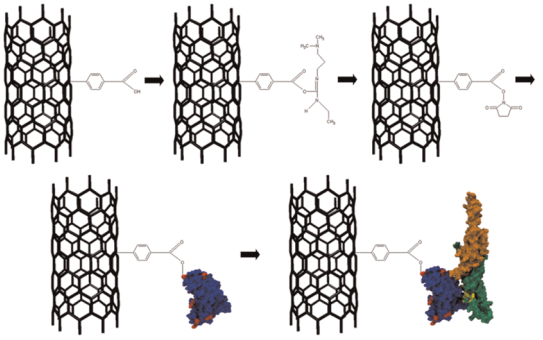

Figure 1. Functionalization scheme for OPN attachment. First, sp^3-hybridized sites are created on the nanotube sidewall by incubation in a diazonium salt solution. The carboxylic acid group is then activated by EDC and stabilized with NHS. ScFv antibody displaces the NHS and forms an amide bond (surface amine-rich lysine residues responsible for this bond are depicted in red), and OPN binds preferentially to the scFv in the detection step. The OPN epitope is shown in yellow, and the C- and N-termini are in orange and green, respectively.

NT-FET-based biosensors. First, scFv can be expressed in a bacterial cell system that improves both the speed and cost of goods associated with their production as compared to traditional IgGs. Second, the scFv is composed entirely of the antigen-binding domain of the 23C3. Thus, antigen binding by an immobilized scFv is hypothesized to bring OPN into closer proximity to the NT-FET surface, as compared to what would occur with an intact IgG. This should result in a greater impact on the electrical properties of the device and potentially improve the sensitivity of detection.

Here we report successful fabrication of NT-FETs covalently functionalized with the 23C3 scFv, as evidenced by atomic force microscopy and electronic measurements. We observed an antigen-specific, concentration-dependent sensor response to OPN in buffer; measured responses from a collection of 10−15 devices could be used to reliably differentiate between pure buffer solution and buffer containing OPN at a concentration of 1 pg/mL, or 30 fM. The response as a function of concentration was well fit by a model based on the Hill−Langmuir equation of equilibrium thermodynamics.

RESULTS AND DISCUSSION

NT-FET devices were fabricated as described in the Methods section. Briefly, NTs were grown by catalytic chemical vapor deposition, and electrical contacts were patterned using a photolithographic technique that is optimized to leave a chemically clean NT sidewall.[27] Pristine sp^2-bonded carbon is chemically inert, so steps must be taken to create a defect on which to bind proteins (Figure 1). An atomic force microscope image of a representative sample and a sample schematic are presented in Supplemental Figure 1 in the Supporting Information. Diazonium salt treatment[28] was used to create sp^3-bonded sites along

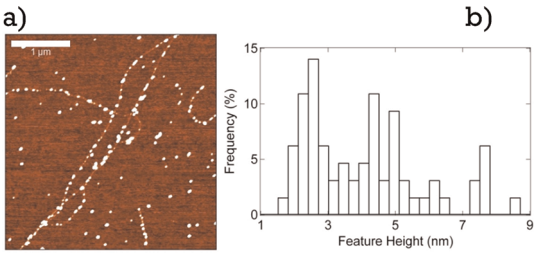

Figure 2. (a) AFM image of scFv antibodies covalently bound to carbon nanotubes, with a typical density of 4−5 attachment sites per micrometer of nanotube length. Scale bar is 1 μm. Height scale is 7 nm. (b) Histogram of the heights of the white features bound to the nanotube in part (a) shows a maximum at ~2.5 nm, consistent with the expected height of scFv antibodies. Secondary maxima at 5 and 7.5 nm are attributed to small aggregates of scFv antibodies. The total number of features analyzed is 180.

the nanotube terminated in a carboxylic acid group that was used for further attachment chemistry. Raman spectroscopy measurements showed an increase in the ratio of the intensity of the D band to the G band after diazonium salt treatment, consistent with the creation of covalent bonds to the NT sidewall (see Supplemental Figure 2 in the Supporting Information).[29]

The diazonium treatment step was followed by activation and stabilization of the attachment site with 1-ethyl-3-[3-dimethylaminopropyl]carbodiimide hydrochloride/sulfo-*N*-hydroxysuccinimide (EDC/NHS).[21] Amine groups associated with lysine residues on scFv proteins were expected to displace NHS in the subsequent attachment step to form a covalent bond between the scFv and the NT through the phenolic linker. A careful washing procedure was employed to minimize scFv binding to the substrate. We expect that the chemical functionalization procedure used here for the scFv derived from the 23C3 mAb[30] may be generalized to broad classes of protein that have a free amine group on their exterior.

Preferential attachment of scFv antibodies to NTs was confirmed by atomic force microscopy (AFM) (Figure 2a). The linear density of attached scFv antibodies was found to be approximately 4−5 per μm of NT length. Line scans from the AFM images were used to calculate the size of ~180 features presumed to be scFv antibodies covalently bound to NTs, and these data were used to form a histogram shown in Figure 2b. The histogram had its maximum at ~2.5 nm, with secondary maxima at 5 and 7.5 nm. We attribute the primary maximum to attachment of single anti-OPN scFv molecules and note that a molecular diameter of 2.5 nm is consistent with their mass of 25 kDa; the other maxima are attributed to small scFv aggregates. We conducted a control experiment to establish that NTs and the NT−SiO_2 interface show very low affinity for nonspecific binding of the scFv and OPN; details are provided in Supplemental Figure 3 of the Supporting Information.

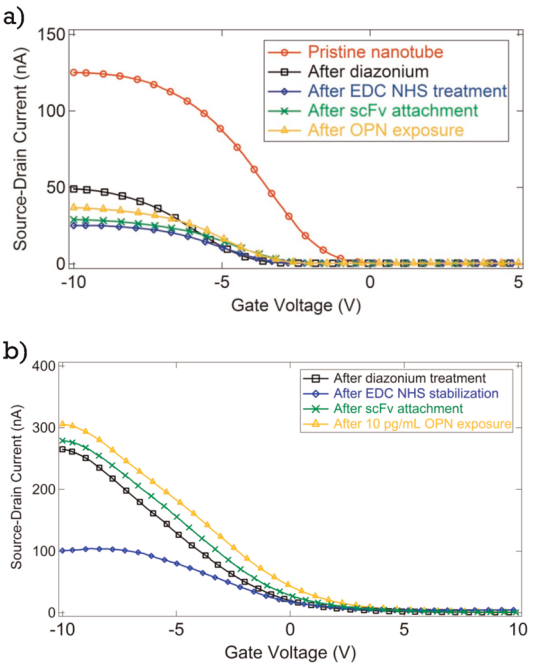

Figure 3. (a) $I-V_g$ characteristics for a single device after successive functionalization steps. Exposure to OPN at a concentration of 30 ng/mL (912 pM) caused the ON state current to increase from 29 nA (green curve) to 37 nA (orange curve), an increase of 27%. (b) Similar data for exposure to OPN at a concentration of 10 pg/mL (304 fM). The ON state current increases from 276 nA to 307 nA, an increase of 11%.

We measured the current−gate voltage ($I-V_g$) characteristic of an individual NT-FET device after each chemical modification to monitor the effect of the chemical functionalization and confirm attachment of scFv antibodies (Figure 3). The most sensitive parameters were the threshold voltage, where the FET current decreases most sharply, and the ON state current carried by the device for very negative values of the gate voltage. The diazonium treatment was found to shift the turn-off voltage by about −3 V, and it reduced the ON state current by 50−90%, consistent with increased electron scattering due to generation of defects on the NT sidewall. EDC/NHS treatment caused almost no change in the turn-off voltage and a slight decrease in the ON state current. ScFv attachment did not change the turn-off voltage and led to a small increase in the ON state current, attributed to a reduction in carrier scattering due to the presence of the protein compared to that associated with NHS/EDC activation.

To test the sensitivity of the device to exposure to OPN, a 10 μL droplet of PBS buffer containing OPN at a known concentration was placed on the sensor and left to incubate for 20 min in a humid environment, followed by careful washing with DI water. The 20-min incubation time we used should allow OPN molecules to diffuse distances on the order of 300 μm, which we expect is sufficient to establish equilibrium between

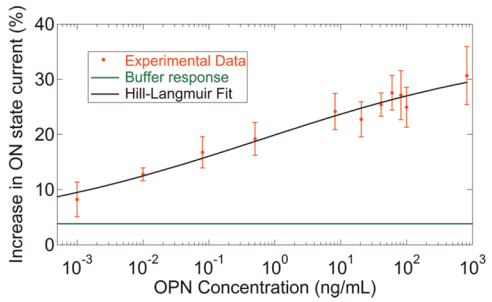

Figure 4. Measured sensor responses over a wide range of concentrations of osteopontin (OPN). The solid line is a fit using a modified Hill−Langmuir expression that includes an offset response of 4% due to the buffer itself (see main text). A clear signal is still present at OPN concentrations of 1 pg/mL.

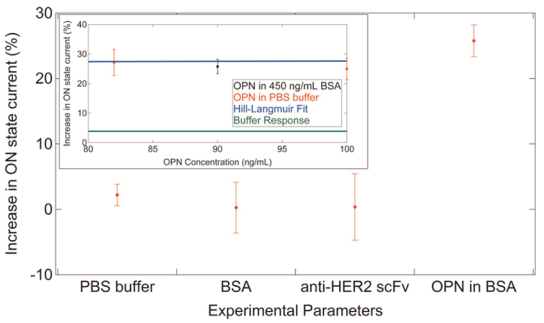

Figure 5. Summary of data from control experiments. Devices exposed to neat PBS buffer showed a response of +4%. Exposure to bovine serum albumin (BSA) at 450 ng/mL gave a null response. Devices prepared with the anti-HER2 scFv antibody in place of anti-OPN scFv and exposed to 90 ng/mL OPN also gave a null response. (Inset) Devices prepared with anti-OPN scFv antibodies and exposed to a mixture of 90 ng/mL OPN and 450 ng/mL BSA background protein gave a response identical to that expected for 90 ng/mL OPN in plain buffer.

bound and unbound species even at the lowest concentration used (1 pg/mL, equal to approximately 30 fM).[31,32] Each device tested was used for a single measurement at a fixed OPN concentration to avoid contamination of the samples. The ON state current proved to be very sensitive to the presence of OPN and showed a reproducible increase after exposure to OPN (Figure 3). The response is reported as $\Delta I/I$, the percentage increase in ON state current from the scFv-functionalized state to the state following OPN exposure, which is found to account well for device-to-device resistance variations.

The device response varied systematically with OPN concentration as shown in Figure 4. Each data point in the plot was generated by averaging the responses of 10−15 functionalized NT-FET devices tested against a solution with the same concentration of OPN; the error bar shown is the standard error of the mean. To generate a fit to the data, we used a model where the device response was composed of two additive components: an offset response, Z, due to incubation in pure buffer with no OPN and a response that is directly proportional to the probability that an OPN binding site is occupied. This motivated a fit based on a modified Hill−Langmuir equation describing ligand−receptor binding in equilibrium.[33]

$$\frac{\Delta I}{I} = A\frac{(c/K_d)^n}{1+(c/K_d)^n} + Z$$

Here c is the OPN concentration, A is the response when all binding sites are occupied, Z is an overall offset to account for the response to pure buffer, K_d is the dissociation constant, and n is the Hill coefficient describing cooperativity of binding. The best fit to the data yielded a maximum response A = 27%, offset parameter Z = 4%, dissociation constant K_d = 560 pg/mL, and n = 0.20. The maximum response A and the offset parameter Z were constrained to values that were sensible based on the response data and buffer response, respectively, while n and K_d were free to vary. The best fit value of the offset parameter Z = 4% was in good agreement with the measured responses of devices to pure buffer ($\Delta I/I$ = 2.2 ± 1.8%; see Figure 5). The value of K_d (17 pM) obtained by the NT-FETs is lower than the value of K_d derived from SPR measurements (290 pM; see Supplemental Figure 4 in the Supporting Information). This difference may be explained by the fact that surface plasmon resonance (SPR) is performed under conditions of buffer flow that preclude rebinding of the OPN to the anti-OPN scFv during the dissociation phase measurements. In contrast, the static conditions used with the NT-FET devices likely allow for rebinding, slowing the effective off-rate and resulting in the lower apparent value of K_d. Interestingly, the values derived from the NT-FET data are equivalent to those predicted for the Hu23C3 mAb derived from ELISA-based methods,[25] which are taken under static conditions similar to the conditions of the experiments described here. The best fit value n = 0.20 indicates negative cooperativity in the binding of OPN to the 23C3 scFv in the context of the NT-FET biosensor. This could be due to inhibition of multiple OPN molecules binding to small aggregates or clusters of scFv due to steric hindrance. The data presented in Figure 4 show that the measured responses from a collection of 10−15 devices could be used to reliably differentiate between pure buffer solution ($\Delta I/I$ = 2.2 ± 1.8%; see Figure 5) and buffer containing OPN at a concentration of 1 pg/mL, or 30 fM ($\Delta I/I$ = 9.0 ± 3.0%).

The precise mechanism for the observed sensing response remains to be determined. Qualitatively, an increase in ON state current implies a reduction in carrier scattering upon OPN binding. One possible explanation is that charged sites on the scFv surface are neutralized by opposite charges associated with bound OPN, leading to reduced fluctuations in the electrostatic potential at the NT surface. OPN is known to be a highly acidic protein, with a predicted pI = 4.2,[34] and is therefore expected to have a net negative

charge in the buffer solution (pH = 7.6). Even in the absence of a quantitative understanding of the device response, our results provide strong evidence that the methods used here enabled attachment of engineered proteins to a NT-FET while maintaining both the high-quality electronic characteristics of the NT device and the chemical recognition functionality characteristic of the protein.

Control experiments were conducted to test the assumption that scFv molecules bound to NT devices with this approach retained specificity for their target antigen. In the first experiment, scFv-functionalized sensors were incubated in a solution of bovine serum albumin (BSA) at high concentration (450 ng/mL) to approximate the effect of nonspecific proteins present in patient samples. The devices were found to give a null response of $-0.24\% \pm 3.87\%$ (Figure 5), supporting the notion that the scFv antibodies bound to the NT sidewall retained their specificity for OPN. In a second test of antigen specificity, we functionalized NT-FET devices with a different scFv based on the clinically validated therapeutic monoclonal antibody trastuzumab.[35] Trastuzumab, and the derived 4D5 scFv, binds to the HER2 receptor tyrosine kinase, which is implicated in breast cancer formation and progression.[35] SPR measurements show that the 4D5 scFv binds to HER2 with a K_D of 1.9 nM,[36] equivalent to the binding affinity of 23C3 for OPN, and they also show that the 4D5 scFv exhibits no binding to OPN (see Supplemental Figure 5 in the Supporting Information). As detailed in Figure 5, 4D5-functionalized devices show no response after exposure to OPN at 100 ng/mL, consistent with the SPR data. We also measured the response of 23C3 scFv-functionalized devices to a mixture of OPN (90 ng/mL) and BSA (450 ng/mL) to partially simulate the complexity characteristic of clinical samples. The sensor response of ~26% was statistically identical to that observed for devices exposed to pure OPN (see Figure 5). These control experiments suggest that anti-OPN 23C3 scFv-functionalized carbon nanotube sensors exhibit a high level of specificity for OPN, the target ligand.

CONCLUSIONS

We demonstrated that biosensor devices composed of high-affinity, engineered antibodies coupled to sensitive carbon nanotube transduction elements were capable of detecting prostate cancer biomarker at concentrations as low as 1 pg/mL (30 fM), 3 orders of magnitude lower than ELISA immunoassays, the current clinical standard.[37] The experiments showed an antigen-specific, concentration-dependent sensor response over a wide range of concentrations (1 pg/mL to 1 μg/mL) that was in excellent quantitative agreement with a model based on the Hill–Langmuir equation of equilibrium thermodynamics. Control experiments indicated that the anti-OPN scFv retains its highly specific binding characteristics when integrated into the hybrid nanostructure. Exposing the sensor to PBS buffer that contained a high concentration of bovine serum albumin did not induce a sensing response, and devices functionalized with 4D5 scFv, which binds specifically to HER2 and not to OPN, did not produce a sensing response upon exposure to OPN. We explored the response of the device to protein mixtures and found that the response to OPN in a concentrated protein background was equal to that measured for OPN in pure buffer. These observations make us optimistic that this device concept may be generalized to many other protein species and is perhaps suitable for translation into a useful tool to help diagnose disease and guide its treatment.

METHODS

Device Fabrication. Silicon (p++ doped) wafers with 500 nm thermally grown oxide were covered with randomly dispersed iron nitrate catalyst. Carbon nanotubes were grown at 900 °C *via* chemical vapor deposition with methane feedstock in an argon/hydrogen reducing atmosphere as published previously.[15] Source and drain electrodes separated by 2.5 μm were patterned photolithographically directly on the carbon nanotube network with a bilayer resist process of PMGI and Shipley 1813 followed by metal deposition (5 nm Ti/40 nm Pd) in a thermal evaporator. Liftoff in acetone and Microposit CD-26 was followed by a brief anneal in Ar/H_2 at 350 °C to remove photoresist residues.[27] Device current–gate voltage ($I-V_G$) characteristics were measured under ambient laboratory conditions. Only carbon nanotube transistors with ON/OFF ratios greater than 100 and differences between turn-on voltage and turn-off voltage less than 6 V were used in subsequent measurements.

Expression and Purification of anti-OPN 23C3 scFv. A gene encoding the 23C3 scFv, in a Vh–linker–Vl orientation, was synthesized based on the publically available amino acid sequence (PDB ID: 3CXD) and with a codon usage bias for expression in *E. coli*. The gene was cloned into the pSYN2 expression vector as an NcoI/XhoI fragment, and the protein was purified to a level of 0.2 mg/L of culture from the periplasmic space of TG1 *E. coli* by sequential Ni-NTA and size exclusion chromatography as previously described.[38] For use as a control, the hu4D5 anti-HER2 scFv corresponding to the FDA-approved mAb trastauzumab was synthesized from the publically available amino acid sequence in a Vl–linker–Vh orientation as previously described,[39] expressed in TG1 *E. coli*, and purified as described for 23C3 scFv.

Functionalization. NT-FETs were first functionalized using 4-carboxybenzene diazonium tetrafluoroborate that we synthesized according to a published recipe.[40] Devices were immersed in diazonium salt solution (2.5 mg/mL deionized water) for 1 h at 40 °C to create multiple sp^3-hybridized sites along the nanotube ending in a carboxylic acid group.[21] After incubation in a water bath, devices were rinsed in acetone, methanol, and DI water. The carboxylic acid groups were then activated and stabilized in a solution of EDC and NHS at concentrations of 6 mg and 16 mg per 15 mL of MES buffer, respectively, for 15 min at room temperature followed by a DI water rinse. A solution of scFv antibodies (1 μg/mL) at pH 7.3 was then pipetted onto the

devices in a humid environment to keep the solution from evaporating, causing NHS-stabilized sites to be displaced by scFv protein over an incubation period of one hour. After incubation with protein solution, chips were dipped in a DI water bath and agitated for 1 min. Chips were then removed and placed in a second DI water bath without drying and agitated again for 1 min. Chips were then blown dry in a gentle (less than 20 psi) stream of nitrogen.

Conflict of Interest: The authors declare no competing financial interest.

Acknowledgment. This research was supported by the Department of Defense U.S. Army Medical Research and Materiel Command through grants W81XWH-09-1-0205 and W81XWH-09-1-0206. We acknowledge support of NIH Core Grant CA06927 (M.K.R.) and use of facilities associated with the Nano/Bio Interface Center, National Science Foundation NSEC DMR08-32802 (A.T.C.J.).

Supporting Information Available: Information concerning the sample geometry, Raman spectra showing the effect of diazonium treatment. Control experiment to exclude nonspecific binding of proteins to NTs. Chemical functionalization of carbon nanotube devices. Surface plasmon resonance analysis of binding affinities of scFvs. This information is available free of charge *via* the Internet at http://pubs.acs.org.

REFERENCES AND NOTES

1. Group, U.S.C.S.W. *United States Cancer Statistics: 1999–2007 Incidence and Mortality Web-Based Report*. U.S. Department of Health and Human Services, C.f.D.C.a.P.a. N.C.I., Ed.; Atlanta, GA, **2010**.
2. Thompson, I. M.; Pauler, D. K.; Goodman, P. J.; Tangen, C. M.; Lucia, M. S.; Parnes, H. L.; Minasian, L. M.; Ford, L. G.; Lippman, S. M.; Crawford, E. D.; *et al*. Prevalence of Prostate Cancer among Men with a Prostate-Specific Antigen Level ≤4.0 Ng Per Milliliter. *N. Engl. J. Med.* **2004**, *350*, 2239–2246.
3. Smith, D. S.; Humphrey, P. A.; Catalona, W. J. The Early Detection of Prostate Carcinoma with Prostate Specific Antigen—The Washington University Experience. *Cancer* **1997**, *80*, 1852–1856.
4. Fedarko, N. S.; Jain, A.; Karadag, A.; Van Eman, M. R.; Fisher, L. W. Elevated Serum Bone Sialoprotein and Osteopontin in Colon, Breast, Prostate, and Lung Cancer. *Clin. Cancer Res.* **2001**, *7*, 4060–4066.
5. Sodek, J.; Ganss, B.; McKee, M. D. Osteoponitn. *Crit. Rev. Oral Biol. Med.* **2000**, *11*, 279–303.
6. Morimoto, J.; Kon, S.; Matsui, Y.; Uede, T. Osteopontin as a Target Molecule for the Treatment of Inflammatory Diseases. *Curr. Drug Targets* **2010**, *11*, 494–505.
7. Bellahcene, A.; Castronovo, V.; Ogbureke, K. U.; Fisher, L. W.; Fedarko, N. S. Small Integrin-Binding Ligand N-Linked Glycoproteins (Siblings): Multifunctional Proteins in Cancer. *Nat. Rev. Cancer* **2008**, *8*, 212–226.
8. Hotte, S. J.; Winquist, E. W.; Stitt, L.; Wilson, S. M.; Chambers, A. F. Plasma Osteopontin: Associations with Survival and Metastasis to Bone in Men with Hormone-Refractory Prostate Carcinoma. *Cancer* **2002**, *95*, 506–512.
9. Fan, K.; Dai, J.; Wang, H.; Wei, H.; Cao, Z.; Hou, S.; Qian, W.; Li, B.; Zhao, J.; Xu, H.; *et al*. Treatment of Collagen-Induced Arthritis with an Anti-Osteopontin Monoclonal Antibody through Promotion of Apoptosis of Both Murine and Human Activated T Cells. *Arthritis Rheum.* **2008**, *58*, 2041–2052.
10. Anborgh, P. H.; Wilson, S. M.; Tuck, A. B.; Winquist, E.; Schmidt, N.; Hart, R.; Kon, S.; Maeda, M.; Uede, T.; Stitt, L. W.; *et al*. New Dual Monoclonal Elisa for Measuring Plasma Osteopontin as a Biomarker Associated with Survival in Prostate Cancer: Clinical Validation and Comparison of Multiple Elisas. *Clin. Chem.* **2009**, *55*, 895–903.
11. Plumer, A.; Duan, H.; Subramaniam, S.; Lucas, F. L.; Miesfeldt, S.; Ng, A. K.; Liaw, L. Development of Fragment-Specific Osteopontin Antibodies and Elisa for Quantification in Human Metastatic Breast Cancer. *BMC Cancer* **2008**, *8*, 38.
12. Ward, A. M.; Catto, J. W.; Hamdy, F. C. Prostate Specific Antigen: Biology, Biochemistry and Available Commercial Assays. *Ann. Clin. Biochem.* **2001**, *38*, 633–651.
13. Gao, X.; Zheng, G.; Lieber, C. M. Subthreshold Regime Has the Optimal Sensitivity for Nanowire Fet Sensors. *Nano Lett.* **2010**, *10*, 547–552.
14. Chen, R. J.; Choi, H. C.; Bangsaruntip, S.; Yenilmez, E.; Tang, X. W.; Wang, Q.; Chang, Y. L.; Dai, H. J. An Investigation of the Mechanisms of Electronic Sensing of Protein Adsorption on Carbon Nanotube Devices. *J. Am. Chem. Soc.* **2004**, *126*, 1563–1568.
15. Staii, C.; Chen, M.; Gelperin, A.; Johnson, A. T. DNA-Decorated Carbon Nanotubes for Chemical Sensing. *Nano Lett.* **2005**, *5*, 1774–1778.
16. Allen, B. L.; Kichambare, P. D.; Star, A. Carbon Nanotube Field-Effect-Transistor-Based Biosensors. *Adv. Mater.* **2007**, *19*, 1439–1451.
17. Heller, I.; Janssens, A. M.; Mannik, J.; Minot, E. D.; Lemay, S. G.; Dekker, C. Identifying the Mechanism of Biosensing with Carbon Nanotube Transistors. *Nano Lett.* **2008**, *8*, 591–595.
18. Star, A.; Gabriel, J. C. P.; Bradley, K.; Gruner, G. Electronic Detection of Specific Protein Binding Using Nanotube FET Devices. *Nano Lett.* **2003**, *3*, 459–463.
19. Kuang, Z. F.; Kim, S. N.; Crookes-Goodson, W. J.; Farmer, B. L.; Naik, R. R. Biomimetic Chemosensor: Designing Peptide Recognition Elements for Surface Functionalization of Carbon Nanotube Field Effect Transistors. *ACS Nano* **2010**, *4*, 452–458.
20. So, H. M.; Park, D. W.; Jeon, E. K.; Kim, Y. H.; Kim, B. S.; Lee, C. K.; Choi, S. Y.; Kim, S. C.; Chang, H.; Lee, J. O. Detection and Titer Estimation of Escherichia Coli Using Aptamer-Functionalized Single-Walled Carbon-Nanotube Field-Effect Transistors. *Small* **2008**, *4*, 197–201.
21. Goldsmith, B. R.; Mitala, J. J.; Josue, J.; Castro, A.; Lerner, M. B.; Bayburt, T. H.; Khamis, S. M.; Jones, R. A.; Brand, J. G.; Sligar, S. G.; *et al*. Biomimetic Chemical Sensors Using Nanoelectronic Readout of Olfactory Receptor Proteins. *ACS Nano* **2011**, *5*, 5408–5416.
22. Kim, S. N.; Rusling, J. F.; Papadimitrakopoulos, F. Carbon Nanotubes for Electronic and Electrochemical Detection of Biomolecules. *Adv. Mater.* **2007**, *19*, 3214–3228.
23. Cao, Q.; Rogers, J. A. Ultrathin Films of Single-Walled Carbon Nanotubes for Electronics and Sensors: A Review of Fundamental and Applied Aspects. *Adv. Mater.* **2009**, *21*, 29–53.
24. Sanchez, S.; Fabregas, E.; Pumera, M. Detection of Biomarkers with Carbon Nanotube-Based Immunosensors. *Methods Mol. Biol.* **2010**, *625*, 227–237.
25. Fan, K.; Zhang, B.; Yang, H.; Wang, H.; Tan, M.; Hou, S.; Qian, W.; Li, B.; Wang, H.; Dai, J.; *et al*. A Humanized Anti-Osteopontin Antibody Protects from Concanavalin a Induced-Liver Injury in Mice. *Eur. J. Pharmacol.* **2011**, *657*, 144–151.
26. Holliger, P.; P.J., H. Engineered Antibody Fragments and the Rise of Single Domains. *Nat. Biotechnol.* **2005**, *23*, 1126–1136.
27. Khamis, S. M.; Jones, R. A.; Johnson, A. T. C. Optimized Photolithographic Fabrication Process for Carbon Nanotube Devices. *AIP Adv.* **2011**, *1*, 022106.
28. Strano, M. S.; Dyke, C. A.; Usrey, M. L.; Barone, P. W.; Allen, M. J.; Shan, H. W.; Kittrell, C.; Hauge, R. H.; Tour, J. M.; Smalley, R. E. Electronic Structure Control of Single-Walled Carbon Nanotube Functionalization. *Science* **2003**, *301*, 1519–1522.
29. Lu, Y.; Lerner, M. B.; Qi, Z. J.; Mitala, J. J.; Lim, J. H.; Discher, B. M.; Johnson, A. T. C. Graphene-Protein Bioelectronic Devices with Wavelength-Tunable Photoresponse. *Appl. Phys. Lett.* **2012**, *100*, 033110.
30. Du, J.; Hou, S.; Zhong, C.; Lai, Z.; Yang, H.; Dai, J.; Zhang, D.; Wang, H.; Guo, Y.; Ding, J. Molecular Basis of Recognition of Human Osteopontin by 23c3, a Potential Therapeutic Antibody for Treatment of Rheumatoid Arthritis. *J. Mol. Biol.* **2008**, *382*, 835–842.

31. Squires, T. M.; Messinger, R. J.; Manalis, S. R. Making It Stick: Convection Reaction and Diffusion in Surface-Based Biosensors. *Nat. Biotechnol.* **2008**, *26*, 417–426.
32. Arlett, J. L.; Myers, E. B.; Roukes, M. L. Comparative Advantages of Mechanical Biosensors. *Nat. Nanotechnol.* **2011**, *6*, 203–215.
33. Hill, A. The Possible Effects of the Aggregation of the Molecules of Hemoglobin on Its Oxygen Dissociation Curve. *J. Physiol.* **1910**, *40*, 4–7.
34. Butler, W. T.; Ridall, A. L.; McKee, M. D. Osteopontin. In *Principals of Bone Biology*; Bilezikian, J. P.; Raisz, L. G.; Rodan, G. A., Eds.; Academic Press: New York, 1996; pp 167−181.
35. Slamon, D. J.; Leyland-Jones, B.; Shak, S.; Fuchs, H.; Paton, V.; Bajamonde, A.; Fleming, T.; Eiermann, W.; Wolter, J.; Pegram, M.; *et al*. Use of Chemotherapy Plus a Monoclonal Antibody against Her2 for Metastatic Breast Cancer That Overexpresses Her2. *N. Engl. J. Med.* **2001**, *344*, 783–792.
36. Worn, A.; Pluckthun, A. An Intrinsically Stable Antibody Scfv Fragment Can Tolerate the Loss of Both Disulfide Bonds and Fold Correctly. *FEBS Lett.* **1998**, *427*, 357–361.
37. MacBeath, G. Protein Microarrays and Proteomics. *Nat. Genet.* **2002**, *32*, 526–532.
38. Robinson, M. K.; Hodge, K. M.; Horak, E.; Sundberg, A. L.; Russeva, M.; Shaller, C. C.; von Mehren, M.; Shchaveleva, I.; Simmons, H. H.; Marks, J. D.; *et al*. Targeting Erbb2 and Erbb3 with a Bispecific Single-Chain Fv Enhances Targeting Selectivity and Induces a Therapeutic Effect *in Vitro*. *Br. J. Cancer* **2008**, *99*, 1415–1425.
39. Kubetzko, S.; Balic, E.; Wiaibel, R.; Zangemeister-Wittke, U.; Pluckthun, A. Pegylation and Multimerization of the Anti-P185 Her-2 Single Chain Fv Fragment 4d5. *J. Biol. Chem.* **2006**, *281*, 35186–35201.
40. Saby, C.; Ortiz, B.; Champagne, G. Y.; Belanger, D. Electrochemical Modification of Glassy Carbon Electrode Using Aromatic Diazonium Salts 0.1. Blocking Effect of 4-Nitrophenyl and 4-Carboxyphenyl Groups. *Langmuir* **1997**, *13*, 6805–6813.

Biomimetic Chemical Sensors Using Nanoelectronic Readout of Olfactory Receptor Proteins

Brett R. Goldsmith,[†] Joseph J. Mitala, Jr.,[‡,§] Jesusa Josue,[⊥] Ana Castro,[∥] Mitchell B. Lerner,[†] Timothy H. Bayburt,[#] Samuel M. Khamis,[△] Ryan A. Jones,[△] Joseph G. Brand,[⊥] Stephen G. Sligar,[#] Charles W. Luetje,[∥] Alan Gelperin,[⊥,▽] Paul A. Rhodes,[△,¶] Bohdana M. Discher,[‡,§] and A. T. Charlie Johnson[†,‡,*]

[†]Department of Physics & Astronomy, University of Pennsylvania, Philadelphia, Pennsylvania 19104, United States, [‡]Nano/Bio Interface Center, University of Pennsylvania, Philadelphia, Pennsylvania 19104, United States, [§]Department of Biochemistry and Biophysics, University of Pennsylvania, Philadelphia, Pennsylvania 19104, United States, [⊥]Monell Chemical Senses Center, Philadelphia, Pennsylvania 19104, United States, [∥]Department of Molecular and Cellular Pharmacology, University of Miami, Miami, Florida 33101, United States, [#]Department of Biochemistry, University of Illinois, Urbana, Illinois 61801, United States, [△]Nanosense, Inc., Redwood City, California 94063, United States, [▽]Princeton Neuroscience Institute, Department of Molecular Biology, Princeton University, Princeton, New Jersey 08544, United States, and [¶]Evolved Machines, LLC, Palo Alto,California 94301, United States

ABSTRACT We have designed and implemented a practical nanoelectronic interface to G-protein coupled receptors (GPCRs), a large family of membrane proteins whose roles in the detection of molecules outside eukaryotic cells make them important pharmaceutical targets. Specifically, we have coupled olfactory receptor proteins (ORs) with carbon nanotube transistors. The resulting devices transduce signals associated with odorant binding to ORs in the gas phase under ambient conditions and show responses that are in excellent agreement with results from established assays for OR–ligand binding. The work represents significant progress on a path toward a bioelectronic nose that can be directly compared to biological olfactory systems as well as a general method for the study of GPCR function in multiple domains using electronic readout.

KEYWORDS: bioelectronics · vapor sensor · olfactory receptor proteins · field effect transistor · nanotube

Integration of modern nanoelectronic technology with the potent molecular machines of living organisms offers a pathway to advanced chemical sensing modalities and high-throughput screening of ligand binding. While significant progress has been made along this path using soluble proteins[1–4] and nucleic acids,[5–7] integration of amphiphilic membrane proteins remains in an early state of development[8–10] despite their vital and varied functionality in living organisms. G-Protein coupled receptors (GPCRs) are a very large family of transmembrane receptors that recognize molecules in the intercellular region and activate important signal transduction pathways. They are involved in many diseases and are important targets for modern drug agents. Olfactory receptor proteins (ORs) are the most numerous class of GPCRs, representing transcription products of ~3% of the mammalian genome.[11] Here we report a method to integrate ORs with carbon nanotube (NT) transistors. Our method includes the formation of a direct chemical bond that localizes the OR within nanometers of the NT device, in contrast to earlier work, where (mobile) membrane proteins were incorporated into a macroscopic lipid bilayer covering the NT transistor. Because of this, we enable direct readout of OR–ligand binding by the NT device.

Efforts to interface nanoelectronic devices to membrane proteins confront challenges due to the hydrophobic nature of their transmembrane domains, which complicates their expression, purification, and solubilization.[12–14] In this work, ORs were purified from cells and then solubilized in two distinct nanoscale constructs: digitonin micelles[12] and engineered, stable, self-assembling nanoscale membrane assemblies known as "nanodiscs".[15] Solubilized ORs were attached *via* a polyhistidine tag (His-tag) to high-quality NT transistors that were previously functionalized with nickel-nitrilotriacetic acid (Ni-NTA).[16]

These advancements in the purification, packaging, and integration of membrane proteins lead to striking improvements in the practical qualities of membrane protein-enabled bioelectronics. This is most dramatically shown in the stability and longevity of the devices, which have demonstrated useful and repeatable sensor functionality over months, instead of the usual day-long, single-experiment lifetime that greatly limits potential applications of current bioelectronics.

* Address correspondence to cjohnson@physics.upenn.edu.

Received for review February 7, 2011 and accepted June 22, 2011.

Published online June 22, 2011
10.1021/nn200489j

TABLE 1. Responses of Mouse Olfactory Receptor Proteins (mORs) to Selected Odorants, in Biological and Electronic Systems[a]

	mOR 174-9			mOR 203-1			mOR 256-17			no OR	
	Xenopus oocyte	micelle nanotube	nanodisc nanotube	HEK	micelle nanotube	nanodisc nanotube	*Xenopus* oocyte	micelle nanotube	nanodisc nanotube	empty micelle	bare NT
eugenol	-8.4	+20.9±4.6	+7.2±1.1	0	+4.0\±0.8	+2.3±1.7	0	+3.0±0.8	+33.6±8.3	+0.5±1.3	0.0±0.2
2-heptanone	0	+4.1±2.2	-3.3±3.4	-4.76	-6.2±1.1	-6.5±1.5	-9.57	-10.5±0.8	-2.1±0.6	-0.7±0.5	+0.6±1.2
heptanal	0	+2.8±1.1	+5.4±3.1	0	-1.1±1.4	-2.2±0.9	-5.30	-3.9±2.0	-0.7±0.6	+1.7±1.7	+0.2±0.6
acetophenone	0	+6.1±0.8	-4.2±1.0	0	-0.1±0.5	-9.6±0.7	-5.93	+0.2±0.7	-2.3±0.8	+1.3±1.2	-0.1±0.1
2,4 DNT	0	+0.2±2.0	-7.7±1.2		-15.0±0.6	-0.7±2.0	-4.67	-2.9±2.7	-23.0±3.1	+0.1±0.7	+0.1±0.1
n-amyl acetate	0	0	-4.4±0.4		-7.4±0.7	-11.0±1.2	0	-16.5±1.0	-3.2±0.5	+0.9±1.4	+0.5±0.6
methyl benzoate	0	+5.6±1.9	-4.2±0.9		-0.9±1.9	-1.6±1.8	0	-3.9±0.8	+2.7±3.4	+0.3±0.6	+0.3±0.7
cyclohexanone	0	-28.2±1.6	-14.9±0.6	0	-14.4±1.5	-10.5±0.4	-1.00	-29.2±1.6	-35.3±3.9	+1.8±3.7	0.0±0.2

[a] For each type of experiment (*Xenopus* oocyte, HEK, and NT device), data are summarized in terms of relative sensing response. Blue indicates little or no response, red indicates a clear, strong response, and purple indicates a moderate response. White boxes represent biological data that are not available. HEK data are from ref 20. mOR-functionalized NT devices respond to odorants that elicit no response from bare NT devices or devices functionalized with empty micelles. Odorant sensitivities of mOR-functionalized NT devices vary with OR identity and are very similar to those seen in *Xenopus* and HEK experiments.

The use of polyhistidine tags and artificial membrane constructs allows precise orientation of the properly folded biological component relative to the transistor readout element. The OR-NT devices detect vapor analytes under ambient conditions, with sensor responses that are reversible, repeatable, and durable. This work thus represents a significant advance beyond earlier reports where membrane proteins coupled to electronic devices were housed in crude membrane fractions[17] or attached to fusion proteins.[18]

Three mouse olfactory receptor proteins (mORs) were selected for overexpression and integration with NT transistors for vapor response testing against a panel of eight odorants: mOR174-9 (also known as mOR-EG) is known to respond to eugenol;[19] mOR203-1 and mOR256-17 respond to 2-heptanone and cyclohexanone, respectively.[20] Two of these mORs (174-9 and 256-17) were screened with a panel of eight odorants using a *Xenopus* oocyte expression system in combination with robotic electrophysiology.[21] The third mOR (203-1) did not express well in the *Xenopus* oocytes; however similar information is available from expression in human embryonic kidney (HEK) cells from others.[20] Table 1 summarizes response characteristics of the three mORs when expressed in heterologous surrogates and also when coupled to the electronic system described in this paper. The response characteristics of ORs are known to be broadly tuned, so that individual ORs recognize a range of different odorants with varying degrees of specificity.[22]

Recombinant mORs were expressed with an N-terminal His-tag in Sf9 insect cells to simplify the purification and guide the attachment of ORs to carbon nanotube devices.[13] After harvesting the cells, target mORs were purified using magnetic beads treated with Ni-NTA. The presence and correct molecular weight of the protein after the purification was verified by Western blot (see Supporting Information). Throughout all stages of the purification process, the protein was maintained in ~4.88 mM (0.6% w/v) digitonin, a surfactant containing a cholesterol-like backbone that promotes functional solubilization of membrane proteins.[12] At concentrations above 0.5 mM, digitonin forms micelles that can house and solubilize individual ORs in a membrane-like environment. In a second approach, ORs were embedded in soluble "nanodiscs", disk-shaped protein–lipid particles designed to self-assemble with well-controlled size and composition.[15,23] Consistent with previous accounts of nanodisc behavior,[24] mOR-nanodiscs exhibited significantly enhanced stability in solution, with a shelf life of several months. In contrast, digitonin-solubilized mORs would aggregate within hours, as confirmed by dynamic light scattering measurements (data not shown); therefore these solutions were used to functionalize NT devices immediately after purification.

Three-terminal transistor circuits that acted as readout elements of OR–odorant binding were fabricated from carbon nanotubes grown on oxidized silicon substrates by catalytic chemical vapor deposition as described previously.[5] Device current–gate voltage (I–V_G) characteristics were measured under ambient laboratory conditions, and circuits with an on/off ratio exceeding 1000 were selected for use in experiments. Devices were functionalized with carboxylated diazonium salts, which readily form covalent bonds to NTs.[25] As detailed in Materials and Methods, a mild diazonium treatment was used, since excessive covalent modification of NTs destroys the semiconducting properties necessary for efficient signal transduction.[16,25] The

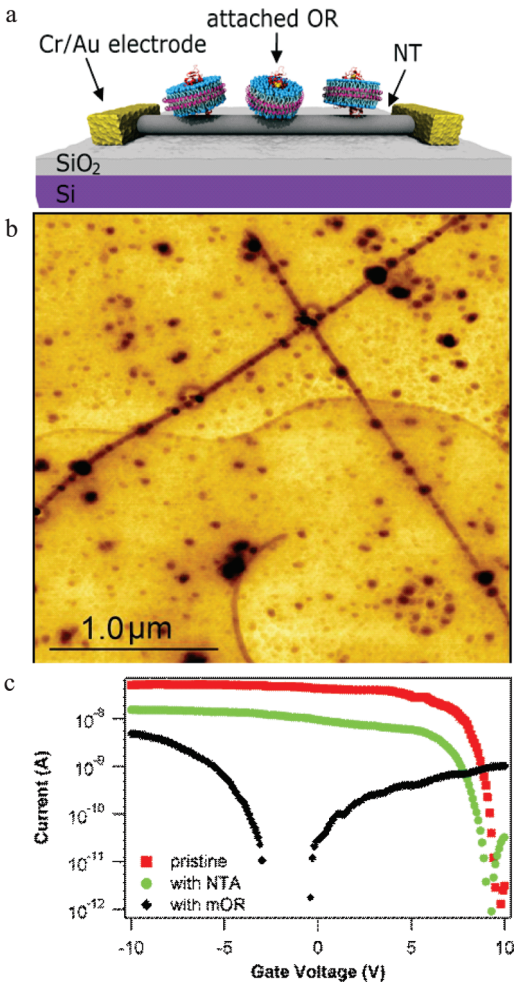

Figure 1. Carbon nanotube devices functionalized with mouse olfactory receptor proteins (mORs). (a) Schematic of a carbon nanotube transistor functionalized with mORs in nanodiscs. (b) AFM image demonstrating preferential attachment of His-tag-labeled mOR 174-9 (darkest circles) in micelles to Ni-NTA-functionalized carbon nanotubes (dark lines). There is strong preference for attachment to the functionalized nanotubes compared to the background. (c) $I-V_G$ curves of the same nanotube device as-fabricated (red), after Ni-NTA functionalization (green), and after incubation in a solution of mORs in digitonin micelles (black). The change in $I-V_G$ associated with Ni-NTA functionalization is consistent with expectations based on association of Ni^{2+} atoms with NTA attached to the nanotube. The change in $I-V_G$ seen after mOR attachment is typical for protein functionalization of nanotube devices. Data were collected with a bias voltage of 100 mV.

carboxylic acid functionality of the diazonium salt was activated with 1-ethyl-3-[3-dimethylaminopropyl]carbodiimide hydrochloride/sulfo-*N*-hydroxysuccinimide (EDC/sNHS) treatment, followed by attachment of the NTA linker. This treatment provides ~5–10 attachment sites for each 1 μm length of exposed nanotube (Figure 1a). Device fabrication was completed with the addition of Ni ions, which are chelated by the NTA complex, and incubation in a solution of mOR-containing digitonin micelles or nanodiscs. This treatment allowed the His-tagged proteins to associate with the Ni-NTA attachment sites. Figure 1b is a schematic of the finished device.

We conducted numerous control experiments using identical incubation and washing protocols to confirm that binding between mORs and the nanotube was controlled by the Ni-NTA:His-tag interaction. We confirmed that empty digitonin micelles and empty nanodiscs have no affinity for Ni-NTA-modified nanotubes. We exposed Ni-NTA-functionalized devices to proteins *without* His-tags and confirmed that no bound proteins remain after the wash protocol. The proteins for the latter experiments were commercially obtained protein G; we did not use the mORs since they were not designed for His-tag removal. All control experiments are thus consistent with the hypothesis of (oriented) protein attachment *via* the expected chemical bond between the Ni-NTA-functionalized nanotube and the protein's His-tag.

Current–gate voltage ($I-V_G$) characteristics were used to monitor the effect of chemical functionalization on performance characteristics of nanotube transistors.[2−5] Figure 1c shows a typical $I-V_G$ curve of an as-fabricated device and its evolution through the functionalization process. We assume that the mechanism underlying changes in NT conduction is dominated by electrostatic coupling to the local environment. Shifts in threshold gate voltage for conduction are attributed to changes in the charge in NT environment, while variation in the on-state current is assumed to reflect changes in carrier scattering. Ni-NTA functionalization leads to a ~3-fold decrease in the on-state current of the NT, which is ascribed to carrier scattering due to covalent attachment of the complex to the NT sidewall. The observed threshold voltage shift of −1 V (from ~10 V to ~9 V) indicates that Ni-NTA functionalization leads to increased positive charge in the nanotube environment, which is associated with the 2+ charge of the nickel ions. Addition of mOR-micelles results in a pronounced decrease in the on-state current and a strong negative shift of the threshold voltage, both consistent with earlier work on protein-functionalized NT transistors.[1−3,14] Similar shifts in threshold and resistance are seen for devices functionalized with mOR-nanodisc constructs.

Responses of NT devices to odorant exposure were measured in a sealed environmental test system through which gas flows of known odorant concentrations were passed (see Materials and Methods). High-purity nitrogen served as a carrier gas for the odorants and to flush the device between exposures to odorant-containing flows. A humidified environment was found to be necessary for device stability, so water vapor was added to all flows to create a relative humidity (RH) of 50%. Devices under test were loaded into the chamber and allowed to equilibrate in a flow of nitrogen at 50% RH. The device was put into the hole conduction regime by setting the back gate voltage 3 V below

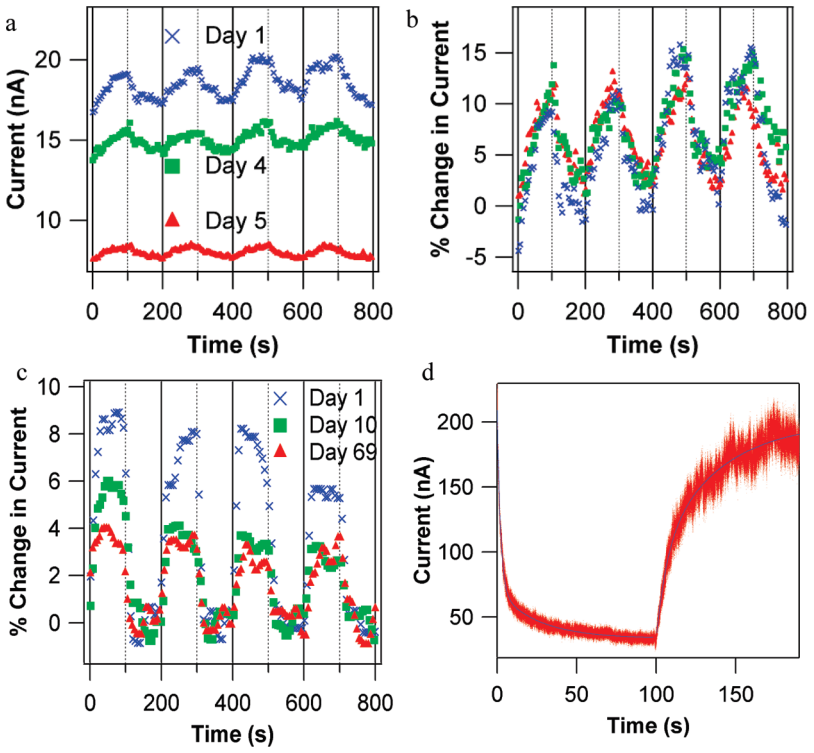

Figure 2. Odorant responses of carbon nanotube (NT) devices functionalized with olfactory receptor proteins (ORs). (a) Three sets of responses to 2 ppm eugenol vapor taken over multiple days using a NT transistor functionalized with mOR174-9 in digitonin micelles. Eugenol vapor is introduced at time 0 and every 200 s (solid vertical lines). The chamber is flushed each time after 100 s of exposure (dashed vertical lines). Although the device baseline current shows significant drift over five days, the normalized current changes are identical, as seen in (b). (c) Characterization of nanodisc packaged OR-NT devices over 10 weeks. The device is based on mOR174-9 in nanodiscs, exposed to 2 ppm eugenol as described in (a). (d) Response to 2250 ppm cyclohexanone and recovery for a NT device functionalized with mOR 256-17 in nanodiscs, with 200 μs resolution. Flow of cyclohexanone begins at time = 0 s, and flow is replaced with clean N_2 at time = 100 s. Red points are raw data, and blue lines are fits based on double-exponential functions. Response time constants are 2.06 $\pm$ 0.1 and 25.51 $\pm$ 0.4 s. Recovery time constants are 6.49 $\pm$ 0.4 and 38.0 $\pm$ 0.2 s. NT device time scales are more rapid than those observed in heterologous expression systems (~2−10 min), where a cellular signal transduction pathway is used to report receptor activation.

the threshold voltage, and the dc resistance was monitored as the device was exposed to gas flows containing odorants for 100 s and then 50% RH nitrogen for 100 s. Five cycles of odorant and carrier gas were used at each odorant concentration to quantify response reproducibility. The response is reported as a fractional change in dc current at constant bias voltage. In NT transistors, changes in resistance due to chemical interactions are caused by shifts in electron scattering or in the effective gating of the transistor, both of which are likely to occur in the odorant−protein−nanotube system.[2,14,26]

Characteristics of odorant responses of mOR-functionalized devices are shown in Figure 2. Large positive responses to eugenol are observed (*i.e.*, increase in device current; Figure 2a,b), consistent with strong responses observed in *Xenopus* oocytes expressing the same OR. NT devices have rapid and reproducible responses and full recovery to baseline, both on second time scales (Figure 2c). As is true for ORs *in vivo*, refreshing the device requires only flushing the odorant from the chamber with carrier gas. As found in previous work with NT-based vapor sensors,[5] differences in device properties can be normalized by presenting sensor responses as a percent change from the baseline current (% $\Delta I/I$).This normalization corrects for device-to-device variation as well as slow drift in a single device over several days (Figure 2b).

After fabrication, micelle devices remained active with stable normalized responses for ~5 days when stored in a humid environment. Devices then became fully inactive and displayed no response to odorant vapors, as was typical of unfunctionalized NT devices (see Table 1). We interpret this degradation as indicative of a breakdown of the digitonin micelle, causing the OR to denature and lose its distinctive odorant-binding properties. In contrast, nanodisc-functionalized devices stored in a humid environment showed ~25% reduction in normalized odorant response over the first several days, but at this point the device responses stabilized with very long lifetimes. Devices showed reproducible responses for longer than one month, with one device maintaining mOR-specific responses to odorants for 10 weeks (Figure 2c). We interpret this result as implying that the nanodisc construct provided a relatively stable environment

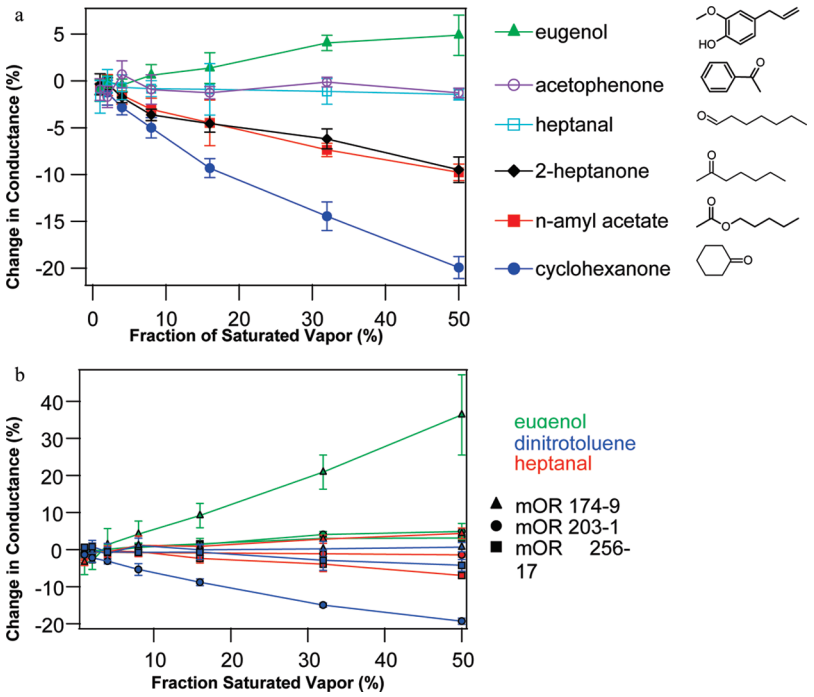

Figure 3. Dependence of device responses upon mOR identity, odorant identity, and odorant concentration. (a) Concentration dependence of responses of NT devices functionalized with mOR203-1 in digitonin micelles to six different odorants. (b) Concentration dependence of the responses for NT devices functionalized with different mORs, tested against eugenol, 2,4-dinitrotoluene, and heptanal. The data demonstrate the diversity of chemical- and concentration-dependent responses seen in the mOR-NT system. Error bars are standard deviation.

for the OR, with only minor degradation over the first few days.

We used a high-speed data acquisition system to investigate the shape and timing of device responses (Figure 2d). We found that response and recovery data are well fit by double-exponential functions (blue lines in Figure 2c), with significant response on time scales < 10 s. The observed time scales are intrinsic to the mOR-NT system, since control experiments indicated that the response time of the apparatus itself is less than 100 ms (Supplemental Figure 4). Response and recovery time scales show little variation with mOR identity, or whether digitonin micelles or nanodiscs were used to solubilize the ORs. Response and recovery are significantly faster than found in heterologous measurements, where a signal transduction pathway is used to report receptor activation, and responses often take several hundreds of seconds.[21]

Responses of OR-functionalized devices were measured for a range of odorants and odorant concentrations. Multiple devices (2−5) were tested for each OR, and the results combined to generate the responses and statistical errors reported in Table 1. Figure 3a shows the concentration dependence of the response of NT devices functionalized with mOR203-1 in digitonin micelles to several odorants, while Figure 3b provides representative examples of how device responses varied with concentration, odorant, and mOR identity. To account for different vapor pressures of the odorants, concentrations are quantified as a fraction of the saturated vapor. Figure 3a shows substantial agreement between the NT device measurements and the HEK data for this mOR, for example, the strong response to 2-heptanone and lack of response to heptanal and acetophenone. Interestingly, the NT device shows nearly identical responses to the chemically similar odorants 2-heptanone and *n*-amyl acetate. The molecules differ only by a single oxygen atom in the functional group attached to a five-carbon chain, and they are perceived as nearly identical by humans.[27] In mice, these two chemicals produce identical neural excitations[28] and olfactory responses,[29] although the interaction of *n*-amyl acetate with the particular mOR 203-1 has not been measured previously. In other cases, odorants with related molecular structures elicit very distinct responses. For example, three odorants in Figure 3a share a carbon ring motif (eugenol, acetophenone, and cyclohexanone), but the odorant responses differ substantially (positive, zero, and negative, respectively).

Similar to other NT-based molecular detection systems, our current understanding of the response mechanism is primarily qualitative. The functionalization chemistry results in the localization of OR-specific binding pockets at distances of a few nanometers from the NT, with a nanoscale hydration layer provided by the humid atmosphere. When odorant molecules are solvated by the hydration layer and bound in the pocket, the conductance of the NT devices is altered, which we assume reflects changes in carrier density

and carrier scattering associated with the electrostatic potential at the NT sidewall. These changes can occur even for the case of uncharged odorant molecules, as is also reported for other sorts of functionalized NT devices.

Of the eight odorants tested, only 2,4-dinitrotoluene is not found in nature. It also produces a response at the lowest concentrations, ~7 ppb, in the range of a "moderately potent" detection threshold for an OR.[30] It is not known whether mice can detect dinitrotoluenes, but there is strong evidence suggesting that they can be sensed by bomb-detecting dogs and rats.[31,32] Mammalian olfactory systems have the ability to detect and categorize new odorants, even those not present during the evolutionary history of the organism, a feature beyond the capability of man-made chemical sensor systems.[22] Our results suggest that the capacity of mORs to bind to nonbiological odorants is preserved when integrated with NT devices, maintaining the mOR's ability to adapt to new analytes. This system thus has potential for the creation of chemical sensor arrays that would have the flexibility of the biological sense of smell; fabrication of such arrays using existing lithography and liquid spotting methods has already been demonstrated (Supplemental Figure 5).

The data indicate that mOR-NT devices have characteristics that are typical of functional ORs *in vivo*, such as the need for a humid environment, the relatively short lifetime of the devices, and the odorant response timing. The data summarized in Table 1 indicate that mOR-NT device responses to odorants show broad agreement with mOR odorant responses found using heterologous techniques for two of the three mORs tested, with only mOR 256-17 showing significant disagreement. Neither the NT nor heterologous systems duplicate the *in vivo* OR response exactly, but areas of agreement between these two test systems strengthen the interpretation of select sensitivities as present in the natural host.

The responses of the devices and the heterologous systems show considerable agreement, although discrepancies exist. For mOR 174-9 and mOR 203-1, all disagreements consist of strong response by the NT device and weak or no response in the heterologous system. Since the NT device responds to all molecules that bind near it, this could reflect odorant binding to the mOR that elicits no cellular response (*e.g.,* an antagonist) or possibly odorant binding not to the mOR but instead to the NT or the digitonin micelle (or nanodisc) that encapsulates the mOR. To exclude the latter possibilities, we conducted control experiments on bare NT transistors and on devices treated with Ni-NTA and empty digitonin micelles (*i.e.*, no mOR; see Table 1). We observed no significant response to any of the tested odorants, with the exception of a small response to cyclohexanone. We infer that observed device responses reflect NT transistor readout of the binding affinity of the attached mORs, with the possible exception of cyclohexanone. This reasoning informs the interpretation of the data for mOR256-17, which shows the broadest set of responses in the heterologous system and poor agreement between the NT and heterologous data. The synthetic membrane environments that we used to house the OR may lead to subtle perturbations to the mOR structure, thereby shuffling the multiple affinities that characterize mOR256-17.

In conclusion, we have successfully developed purification, solubilization, and biofunctionalization schemes that enable control of the bionano interface between olfactory receptor (membrane) proteins and carbon nanotubes. Vapor response measurements demonstrate that ORs with known odorant sensing properties can be coupled to an electronic device and transfer many of those sensing properties to the device. Future work exploring additional ORs and other types of GPCRs could help to understand differences between protein–nanotube measurements, heterologous measurements, and *in vivo* measurements. Conceptually, this opens up a very large domain of intra- and intercellular communication to electronic eavesdropping and could serve as a powerful tool for molecular and cell biology research.

MATERIALS AND METHODS

Electrophysiological Characterization of Mouse Olfactory Receptors Expressed in *Xenopus* Oocytes. We refer to mORs using the nomenclature of Zhang and Firestein.[33] Receptor coding regions were cloned into the pCI expression vector (Promega) containing an N-terminal extension consisting of the N-terminal 20 amino acid residues of human rhodopsin. Receptors were co-expressed with human Ga_{olf} and the human cystic fibrosis transmembrane regulator (CFTR), serving as a reporter channel.

Oocytes were surgically removed from mature *Xenopus laevis* frogs (Nasco). Follicle cells were removed by treatment with collagenase B (Boehringer Mannhem) for 2 h at room temperature. Oocytes were injected with cRNA in 23 nL of water. cRNA quantities injected per oocyte: mORs, 25 ng; Ga_{olf}, 10 ng, CFTR, 1 ng. Oocytes were incubated at 18 °C in Barth's saline (in mM: 88 NaCl, 1 KCl, 2.4 $NaHCO_3$, 0.3 $CaNO_3$, 0.41 $CaCl_2$, 0.82 $MgSO_4$, 15 HEPES, pH 7.5 and 12 μg/mL tetracycline) for 2–4 days prior to electrophysiological recording.

Odorant-induced Cl^- currents, resulting from cAMP-mediated activation of the co-expressed CFTR reporter channel, were measured 2–4 days after cRNA injection using a two-electrode voltage clamp in an automated parallel electrophysiology system (OpusExpress 6000A, Molecular Devices). Oocytes were perfused with ND96 (96 mM NaCl, 2 mM KCl, 1 mM $CaCl_2$, 1 mM $MgCl_2$, 5 mM HEPES, pH 7.5). Micropipets were filled with 3 M KCl and had resistances of 0.2–2.0 MΩ. The holding potential was −70 mV. Current responses, filtered (4-pole, Bessel, low pass) at 20 Hz (−3 db) and sampled at 100 Hz, were captured and stored using OpusXpress 1.1 software (Molecular Devices).

Analysis was done using Clampfit 9.1 software (Molecular Devices).

Our electrophysiological results for mOR256-17 are at some variance with published reports[20] that mOR256-17 responds to cyclohexanone, but not to heptanal or 2-heptanone. We obtained the mOR256-17 expression construct from the Matsunami laboratory[20] and found that, in our hands, this construct yields results in agreement with what we show in Figure 1 in this paper. Similarly, when the Matsunami laboratory retested their mOR256-17 expression construct in their assay system, they obtained results in agreement with our results (Dr. Hiroaki Matsunami, personal communication).

Mouse Olfactory Receptor Expression in SF9 Cells. *a. mOR 174-9 and mOR 203-1.* Recombinant mouse olfactory receptors (mOR) 174-9 and 203-1 were expressed in an Sf9 insect cell system using the BaculoDirect Expression System (Invitrogen). The entry clones for mOR 174-9 (Olfr73; BC141607) and 203-1 (Olfr992; BC141642) were from Invitrogen. The DNA sequence of each receptor was verified using primer pairs specific to each receptor. The DNA sequences of both mOR 174-9 and mOR 203-1 clones were verified using GW1 forward primer (GTTGCAACAAATTGATGAGCAATGC) and GW2 reverse primer (GTTGCAACAAATTGATGAGCAATTA).

The entry clones were used to create an expression clone for each mOR through linear recombination reaction using BaculoDirect Linear DNA with an N-terminal His-tag. Two recombinant expression clones were created: mOR 174-9 with N-terminal His-tag, and mOR 203-1 with N-terminal His-tag. All expression clones were used individually to transfect Sf9 insect cells. Six days after transfection, the cells demonstrated signs of infectivity. The viral stock was collected and was labeled P1 viral stock. The P1 viral stock was stored at ~80 °C in the dark with 10% fetal bovine serum (FBS) to protect the recombinant virus from proteases. Second and third rounds of viral amplification were performed and labeled P2 and P3 viral stocks, respectively. An aliquot of P3 viral stock was collected and used to isolate and purify the viral DNA for PCR to check the orientation of the mOR DNA fragment after transfection and expression.

The viral titer of all P3 viral stocks was determined following the protocol on the BacPAK Baculovirus Rapid Titer Kit (Clontech). Once the viral titer was known, Baculovirus Infected Insect Cell (BIIC) stock was prepared for each recombinant mOR. BIIC stock was found to be more stable than the viral stock. BIIC stock with a multiplicity of infection (MOI) of 3 was prepared on the basis of existing methodology.[34] Sf9 cell cultures were infected with BIIC stock to express the recombinant mORs. The expression of all recombinant mORs was monitored by determining the percent viability, total cell density, and viable cell density during the infection process. A decrease in percent viability and increase in both the cell diameter and viral titer can be observed during infection. While still in their log growth phase state, the cells were harvested, as the percent viability of the Sf9 culture reached 70−80%. Cells were harvested by centrifugation (1000*g*, 10 min, 4 °C).

b. mOR 256-17. moR256-17 clone was placed in frame into pFastBac HT (Invitrogen) between *Eco*RI and *Not*I using common procedures for SF9 insect cells.[35] Colonies were screened by PCR. Virus was generated using the Bac-to-Bac system (Invitrogen) according to the manufacturer's instructions. Virus was quantified by plaque assay. For protein production cells were grown in shaker flasks at 125 rpm at 27 °C either in Grace's supplemented medium with 10% FBS or in SF900II medium with 2% FBS. Media also contained 0.25 mg/L amphotericin B (Sigma A9528), 20 mg/L gentamicin (Gibco 15750-060), and 0.1% Pluronic F-68 (Sigma P5556). Cells were infected at a MOI of 1 at a cell density of (1−2) × 10^6 cells/mL. Cells were harvested 48 h post-infection, weighed, frozen in liquid nitrogen, and stored at −80 °C. Expression was confirmed by Western blot using antipentahistidine primary antibody (Qiagen).

Purification of mORs for Incorporation into Digitonin Micelles. *a. Preparation of the Crude Plasma Membrane Fraction (CMF.* Cell pellets were washed initially by resuspending in a concentration of phosphate-buffered saline (PBS) equivalent to the osmolality of the cell growth media and centrifuged (1000*g*, 10 min, 4 °C). The pellets were resuspended in a lysis buffer consisting of 20 mM Tris-HCl (pH 8.0), 1 mM EDTA, 1 mM EGTA, 0.4% (v/v) ethanol, 0.1 mM phenylmethanesulfonyl fluoride, and protease inhibitor cocktail designed for Sf9 cells (Sigma) and homogenized with a Dounce homogenizer (pestle A, 0.0030−0.0060 in.). In some cases, such as when there was a large amount of nuclei present in the homogenate (as evident from the presence of a clear jelly-like substance), the homogenized cell suspension was centrifuged (300*g*, 10 min, 4 °C) to remove the more dense nuclei and unbroken cells. The homogenate, or supernatant in the case of the latter, was then centrifuged (40000*g*, 20 min, 4 °C) and the supernatant discarded. The pellets were resuspended in a solution of 20 mM Tris-HCl (pH 8.0), 3 mM $MgCl_2$, 0.5 mM $CaCl_2$, and 10 μg/mL deoxyribonuclease (DNase)-I and centrifuged (40000*g*, 20 min, 4 °C). The supernatant was discarded, and the pellet was resuspended in approximately 400 μL of 20 mM Tris-HCl (pH 8.0), 3 mM $MgCl_2$, 0.5 mM $CaCl_2$, and 10 μg/mL DNase-I per 30 mL of cells harvested (ca. 0.75 mg total protein/mL cells harvested), using a 5 mL Wheaton homogenizer. Resuspended pellets were then aliquoted into Eppendorf tubes, flash frozen in liquid nitrogen, and stored at −80 °C.

b. mOR Purification Using Nickel-Magnetic Beads. A 400 μL aliquot of CMF was solubilized in a solution such that its final composition was 6.76 mM digitonin, 19 mM NaH_2PO_4, 115 mM NaCl, 12 mM Tris, 2 mM $MgCl_2$, 0.3 mM $CaCl_2$, and 6.2 μg/mL DNase-I. Solubilization of the CMF was achieved *via* agitation on a benchtop vertical rotator for 1 h or *via* sonication with a microtip (Misonix Ultrasonic Liquid Processor). PureProteome nickel-magnetic beads (Millipore) were added to the solubilized CMF in a volume of 50 mM NaH_2PO_4 and 300 mM NaCl, pH 8.0, such that the final concentration of digitonin was 4.88 mM. The Ni-magnetic beads were mixed with solubilized CMF for 1 h at 4 °C on a vertical rotator and isolated with a magnet. The His-tagged protein was eluted from the beads with approximately 1.25 mL of 4.88 mM digitonin prepared with 100 mM acetate buffer (pH 4.0), and the pH was adjusted to 8.0 using a micropH electrode. The pH adjustment typically required no more than 0.2 mL of NaOH. Note: Although the elution of the His-tagged protein from the magnetic beads was not 100% efficient, we obtained significant amounts of protein to see it on Western blots and to perform our sensing experiments.

Purification of mORs for Incorporation into Nanodiscs. A cell pellet was thawed on ice. Cells were resuspended (2.5 mL per gram cells) in ice-cold PBS (Biowhittaker, without magnesium or calcium) containing Roche complete protease inhibitors without EDTA and Sigma inhibitor cocktail (Sigma, P8849). Cells were sonicated on ice using a Branson 450 sonifier at power 5, 80% duty cycle using a microprobe tip with eight 15 s bursts, waiting 30 s between bursts. The sample was centrifuged at 40k rpm in a Ti70 rotor at 4 °C for 30 min. Ice-cold PBS containing protease inhibitors and 2% w/v Fos-choline 12 (Anatrace) was added to the pellet, 2.5 mL per gram of cell starting material, and the sample was agitated in a Falcon tube at 4 °C for 2.5 h. The sample was then centrifuged as before and supernatant loaded onto a 5 mL nickel-chelating FF cartridge (GE Healthcare) in a cold room. The cartridge was washed with three volumes of PBS containing 20 mM imidazole (pH 7.4) and 0.4% w/v Fos-choline 12. Protein was eluted with PBS containing 500 mM imidazole (pH 7.4) and 0.4% w/v Fos-choline 12. Protein-containing fractions were pooled and protein content was measured using Coomassie Plus reagent (Pierce) with bovine serum albumin as standard.

Assembly of mOR Nanodiscs. Nanodiscs were assembled essentially as described previously.[36] Briefly, MSP1E3D1(−) without a polyhistidine tag was mixed with a 0.2 M POPC/0.4 M cholate mixture prepared as described[36] at a ratio of 140 mol POPC to one MSP1E3D1. Fos-choline 12 was added to a final concentration of 0.4%. Olfactory receptor was added to the MSP lipid mixture at a ratio of 1 mg of crude OR per 20 mg of MSP1E3D1 (MW 32 700). Protease inhibitor was added (Roche Complete without EDTA), and detergent was removed at 4 °C with overnight agitation in the presence of an equal volume of moist Amberlite XAD-2, prepared as described.[36] After removal of beads the sample was filtered using a 0.22 μm syringe filter and stored at 4 °C.

Carbon Nanotube Transistor Fabrication. Carbon nanotubes were grown on p++-doped silicon wafers (4 in. diameter) with

500 nm thermal oxide from Silicon Valley Microelectronics. Approximately 5 mL of 50 mg/L iron nitrate solution was spun onto wafers at 2000 rpm until dry to provide growth catalyst. Wafers were broken into halves and annealed at 910 °C for 15 min. Growth was performed in a 50 mm tube furnace at 910 °C in a flow of 2500 standard cubic centimeters per minute (sccm) methane and 320 sccm hydrogen with 600 sccm argon as carrier gas for 10 min. The furnace temperature was then decreased to 100 °C over approximately 2 h in a flow of 320 sccm hydrogen with 600 sccm argon before samples were removed from the furnace.

Nanotube transistor fabrication was carried out using optical lithography. Polymethylglutarimide (PMGI) (Microchem SFS2) was spun on at 4000 rpm for 45 s, and samples were baked at 150 °C for 5 min. Photoresist (Shipley 1813) was spun on at 5000 rpm for 45 s, and samples were baked at 115 °C for 1 min. After an exposure of about 100 mW/cm^2, Microposit MF-319 was used to develop devices for around 1 min.

Chrome (5 nm) and 50 nm gold were deposited in a home-built thermal evaporator. Liftoff was done in an acetone bath, followed by a bath in Microposit Remover-PG to remove the PMGI, then multiple clean water baths.

The resulting devices have a 2 μm source−drain separation. Before electrical measurement, chips were baked at 250 °C in air for 30 min to remove any polymeric residue from fabrication.

Typical nanotubes are single walled, with a diameter of 1.0−2.5 nm. Typical devices have one to three nanotubes bridging the gold electrodes. Electrical data, using the silicon wafer as a transistor back-gate, are gathered on all devices before chemical modification. Devices showing on/off ratios exceeding 1000 were selected for use in experiments.

Chemical (Ni-NTA) Modification of Carbon Nanotubes. Carbon nanotube transistors on silicon wafers were chemically functionalized using a procedure similar to that described previously.[37] All solutions were prepared using deionized water with an electrical resistance of 18.2 MΩ-cm. All chemical modifications were performed on the chips in 50 mL polypropylene Falcon tubes. First, samples were placed in a solution of 10.76 mM 4-carboxybenzene diazonium tetrafluoroborate at 45 °C for 1 h, followed by washing with acetone, methanol, and water. The chips were then placed in a solution of 2 mM EDC and 5 mM Sulfo-NHS, prepared with activation buffer (0.1 M 2-(*N*-morpholino)ethanesulfonic acid sodium salt, 0.5 M NaCl, pH adjusted to 6.0 with HCl) at room temperature for 15 min to activate the carboxylic acid of the 4-carboxybenzene covalently attached to the nanotubes. Immediately afterward, the chips were briefly bathed in activation buffer and placed in a solution of 11.3 mM N_α,N_α-bis(carboxymethyl)-L-lysine hydrate (NTA-NH_2) prepared with PBS (0.1 M NaH_2PO_4, 0.15 M NaCl, pH adjusted to 7.35 with NaOH) for 2 h. Upon completion, the chips were washed with water and placed in a solution of 11.3 mM $NiCl_2$. After 1 h, the chips were removed from the $NiCl_2$ solution, washed with water, and stored in 25% (v/v) ethanol, at 4 °C.

Attachment of mORs to Ni-NTA-Modified Nanotubes. Chips containing Ni-NTA-modified nanotubes were removed from storage in ethanol, rinsed in water, and dried in a stream of high-purity nitrogen or argon gas. A solution containing mORs in digitonin micelles or nanodiscs, prepared as described above, was deposited on the surface of the chips for 30 min, at room temperature. A large enough volume was deposited on the chips such that any volume change over the 30 min period due to evaporation was negligible. If the solution contained surfactant-stabilized mORs, the chips were then rinsed with a 1 mM digitonin solution. If the solution contained mORs in nanodiscs, the chips were rinsed with deionized water. All samples were dried in a stream of nitrogen or argon gas (with the exception of the sample shown in Supplemental Figure 1b, which was air-dried to show the CNT-micelle interaction).

Apparatus for Measuring Response of NT Devices to Odorant Vapors. The procedure for these measurements is as described in ref 38. The temperature, humidity, flow rate, and flow paths are controlled by a computer. The computer also communicates with and controls a Keithley 6485 picoammeter that measures the current through the device. A digital acquisition card provides the 100 mV source−drain voltage and is connected to the analogue out of the Keithley 6485 to record high time resolution current data. The gate is controlled by a Keithley 617 programmable electrometer.

MKS 1179A style mass flow controllers are used to create three flows of nitrogen. One steady flow of 1000 sccm is bubbled through water to provide a humidified stream of gas. The second "sample flow" is switched between a bubbler containing the odorant being tested and a bypass that is not exposed to any odorant. The last flow serves as a "background" to further dilute the sample flow. The "sample" and "background" flows are set so that they add up to a total flow of 1000 sccm. These three flows (humidity, sample, and background) are combined and then fed into the sensing chamber. Throughout the measurement, the total flow rate, temperature, and humidity do not change.

The devices sit in a stainless steel sensing chamber, with gold pogo pin contacts to the interrogated devices. The total volume of the sensing chamber is around 40 mL. Before the measurements, tubing, fittings, valves, and the chamber are cleaned by rinsing with acetone, isopropyl alcohol, and water, followed by baking for 1 h at 150 °C.

Chemical Analytes. All odorants used are liquids under ambient conditions except for 2,4-dinitrotoluene, which is a solid. Carrier gas was bubbled through liquid odorants and forced through a column containing compressed powder of 2,4-dinitrotoluene. Analytes were used in pure form.

All odorants were purchased from Alfa Aesar except for *n*-amyl acetate, which was purchased from Sigma Aldrich.

Acknowledgment. This work was supported by the DARPA RealNose project. Support from the Nano/Bio Interface Center (NSF NSEC DMR08-32802) is gratefully acknowledged, as is use of its facilities. M.L. acknowledges support from the Department of Defense PCRP #PC080542P1.

Supporting Information Available: Information concerning chemical functionalization of carbon nanotube devices. Western blot analysis of receptor purification. Additional data on odorant responses of mOR-NT devices. Control experiment to determine the response time of the measurement apparatus. Experiment with an array of mOR-NT devices. This information is available free of charge *via* the Internet at http://pubs.acs.org.

REFERENCES AND NOTES

1. Star, A.; Gabriel, J. C. P.; Bradley, K.; Gruner, G. Electronic Detection of Specific Protein Binding Using Nanotube FET Devices. *Nano Lett.* **2003**, *3*, 459–463.
2. Zhang, Y. B.; Kanungo, M.; Ho, A. J.; Freimuth, P.; van der Lelie, D.; Chen, M.; Khamis, S. M.; Datta, S. S.; Johnson, A. T. C.; Misewich, J. A.; Wong, S. S. Functionalized Carbon Nanotubes for Detecting Viral Proteins. *Nano Lett.* **2007**, *7*, 3086–3091.
3. Goldsmith, B. R.; Coroneus, J. G.; Khalap, V. R.; Kane, A. A.; Weiss, G. A.; Collins, P. G. Conductance-Controlled Point Functionalization of Single-Walled Carbon Nanotubes. *Science* **2007**, *315*, 77–81.
4. Chen, R. J.; Bangsaruntip, S.; Drouvalakis, K. A.; Kam, N. W. S.; Shim, M.; Li, Y. M.; Kim, W.; Utz, P. J.; Dai, H. J. Noncovalent Functionalization of Carbon Nanotubes for Highly Specific Electronic Biosensors. *Proc. Nat. Acad. Sci. U. S. A.* **2003**, *100*, 4984–4989.
5. Staii, C.; Chen, M.; Gelperin, A.; Johnson, A. T. DNA-Decorated Carbon Nanotubes for Chemical Sensing. *Nano Lett.* **2005**, *5*, 1774–1778.
6. Zuniga, C.; Rinaldi, M.; Khamis, S. M.; Johnson, A. T.; Piazza, G. Nanoenabled Microelectromechanical Sensor for Volatile Organic Chemical Detection. *Appl. Phys. Lett.* **2009**, *94*, 223122.
7. Tang, X. W.; Bansaruntip, S.; Nakayama, N.; Yenilmez, E.; Chang, Y. L.; Wang, Q. Carbon Nanotube DNA Sensor and Sensing Mechanism. *Nano Lett.* **2006**, *6*, 1632–1636.
8. Zhou, X.; Moran-Mirabal, J. M.; Craighead, H. G.; McEuen, P. L. Supported Lipid Bilayer/Carbon Nanotube Hybrids. *Nat. Nanotechnol.* **2007**, *2*, 185–190.

9. Misra, N.; Martinez, J. A.; Huang, S.-C. J.; Wang, Y.; Stroeve, P.; Grigoropoulos, C. P.; Noy, A. Bioelectronic Silicon Nanowire Devices Using Functional Membrane Proteins. *Proc. Nat. Acad. Sci. U. S. A.* **2009**, *106*, 13780–13784.
10. Huang, S.-C. J.; Artyukhin, A. B.; Misra, N.; Martinez, J. A.; Stroeve, P. A.; Grigoropoulos, C. P.; Ju, J.-W. W.; Noy, A. Carbon Nanotube Transistor Controlled by a Biological Ion Pump Gate. *Nano Lett.* **2010**, *10*, 1812–1816.
11. Filmore, D. It's a GPCR World. *Mod. Drug Discovery* **2004**, *7*, 24–28.
12. Hulme, E. C.; Birdsall, N. J. M., *Receptor Biochemistry: A Practical Approach*. IRL Press at Oxford University Press: Oxford, New York, 1990; pp xxi, 326.
13. Raming, K.; Krieger, J.; Strotmann, J.; Boekhoff, I.; Kubick, S.; Baumstark, C.; Breer, H. Cloning and Expression of Odorant Receptors. *Nature* **1993**, *361*, 353–356.
14. Zhou, X. J.; Moran-Mirabal, J. M.; Craighead, H. G.; McEuen, P. L. Supported Lipid Bilayer/Carbon Nanotube Hybrids. *Nat. Nanotechnol.* **2007**, *2*, 185–190.
15. Bayburt, T. H.; Grinkova, Y. V.; Sligar, S. G. Self-Assembly of Discoidal Phospholipid Bilayer Nanoparticles with Membrane Scaffold Proteins. *Nano Lett.* **2002**, *2*, 853–856.
16. Graff, R. A.; Swanson, T. M.; Strano, M. S. Synthesis of Nickel-Nitrilotriacetic Acid Coupled Single-Walled Carbon Nanotubes for Directed Self-Assembly with Polyhistidine-Tagged Proteins. *Chem. Mater.* **2008**, *20*, 1824–1829.
17. Kim, T. H.; Lee, S. H.; Lee, J.; Song, H. S.; Oh, E. H.; Park, T. H.; Hong, S. Single-Carbon-Atomic-Resolution Detection of Odorant Molecules Using a Human Olfactory Receptor-Based Bioelectronic Nose. *Adv. Mater.* **2009**, *21*, 91–94.
18. Yoon, H.; Lee, S. H.; Kwon, O. S.; Song, H. S.; Oh, E. H.; Park, T. H.; Jang, J. Polypyrrole Nanotubes Conjugated with Human Olfactory Receptors: High-Performance Transducers for FET-Type Bioelectronic Noses. *Angew. Chem., Int. Ed.* **2009**, *48*, 2755–2758.
19. Kajiya, K.; Inaki, K.; Tanaka, M.; Haga, T.; Kataoka, H.; Touhara, K. Molecular Bases of Odor Discrimination: Reconstitution of Olfactory Receptors That Recognize Overlapping Sets of Odorants. *J. Neurosci.* **2001**, *21*, 6018–6025.
20. Saito, H.; Chi, Q. Y.; Zhuang, H. Y.; Matsunami, H.; Mainland, J. D. Odor Coding by a Mammalian Receptor Repertoire. *Sci. Signalling* **2009**, *2*, ra9.
21. Abaffy, T.; Matsunami, H.; Luetje, C. W. Functional Analysis of a Mammalian Odorant Receptor Subfamily. *J. Neurochem.* **2006**, *97*, 1506–1518.
22. Albert, K. J.; Lewis, N. S.; Schauer, C. L.; Sotzing, G. A.; Stitzel, S. E.; Vaid, T. P.; Walt, D. R. Cross-Reactive Chemical Sensor Arrays. *Chem. Rev.* **2000**, *100*, 2595–2626.
23. Denisov, I. G.; Grinkova, Y. V.; Lazarides, A. A.; Sligar, S. G. Directed Self-Assembly of Monodisperse Phospholipid Bilayer Nanodiscs with Controlled Size. *J. Am. Chem. Soc.* **2004**, *126*, 3477–3487.
24. Bayburt, T. H.; Sligar, S. G. Membrane Protein Assembly into Nanodiscs. *FEBS Lett.* **2010**, *584*, 1721–1727.
25. Bahr, J. L.; Yang, J. P.; Kosynkin, D. V.; Bronikowski, M. J.; Smalley, R. E.; Tour, J. M. Functionalization of Carbon Nanotubes by Electrochemical Reduction of Aryl Diazonium Salts: A Bucky Paper Electrode. *J. Am. Chem. Soc.* **2001**, *123*, 6536–6542.
26. Heller, I.; Janssens, A. M.; Mannik, J.; Minot, E. D.; Lemay, S. G.; Dekker, C. Identifying the Mechanism of Biosensing with Carbon Nanotube Transistors. *Nano Lett.* **2008**, *8*, 591–595.
27. Wise, P. M.; Olsson, M. J.; Cain, W. S. Quantification of Odor Quality. *Chem. Senses* **2000**, *25*, 429–443.
28. Schwende, F. J.; Wiesler, D.; Novotny, M. Volatile Compounds Associated with Estrus in Mouse Urine - Potential Pheromones. *Experientia* **1984**, *40*, 213–215.
29. Xu, F. Q.; Schaefer, M.; Kida, I.; Schafer, J.; Liu, N.; Rothman, D. L.; Hyder, F.; Restrepo, D.; Shepherd, G. M. Simultaneous Activation of Mouse Main and Accessory Olfactory Bulbs by Odors or Pheromones. *J. Comp. Neurol.* **2005**, *489*, 491–500.
30. Pevsner, J.; Trifiletti, R. R.; Strittmatter, S. M.; Snyder, S. H. Isolation and Characterization of an Olfactory Receptor Protein for Odorant Pyrazines. *Proc. Nat. Acad. Sci. U. S. A.* **1985**, *82*, 3050–3054.
31. Furton, K. G.; Myers, L. J. The Scientific Foundation and Efficacy of the Use of Canines as Chemical Detectors for Explosives. *Talanta* **2001**, *54*, 487–500.
32. Cox, C.; Weetjens, B.; Machangu, R.; Billet, M.; Verhagen, R. Rats for Demining: An Overview of The APOPO Program. *Proceedings of the Eudem Conference on Humanitarian Landmine Detection Technologies*; 2005, 5 pp.
33. Zhang, X. M.; Rogers, M.; Tian, H. K.; Zhang, X. H.; Zou, D. J.; Jian, L.; Ma, M. H.; Shepherd, G. M.; Firestein, S. J. High-Throughput Microarray Detection of Olfactory Receptor Gene Expression in the Mouse. *Proc. Nat. Acad. Sci. U. S. A.* **2004**, *101*, 14168–14173.
34. Wasilko, D. J.; Lee, S. E.; Stutzman-Engwall, K. J.; Reitz, B. A.; Emmons, T. L.; Mathis, K. J.; Bienkowski, M. J.; Tomasselli, A. G.; Fischer, H. D. The Titerless Infected-Cells Preservation and Scale-up (Tips) Method for Large-Scale Production of No-Sensitive Human Soluble Guanylate Cyclase (Sgc) from Insect Cells Infected with Recombinant Baculovirus. *Protein Expr. Purif.* **2009**, *65*, 122–132.
35. Sambrook, J.; Fritsch, E. F.; Maniatis, T. *Molecular-Cloning - a Laboratory Manual*: Cold Spring Harbor Laboratory Press: New York, 1989; Vol. 1.
36. Ritchie, T. K.; Grinkova, Y. V.; Bayburt, T. H.; Denisov, I. G.; Zolnerciks, J. K.; Atkins, W. M.; Sligar, S. G. Reconstitution of Membrane Proteins in Phospholipid Bilayer Nanodiscs. *Methods Enzymol.; Liposomes, Part F* **2009**, *464*, 211–231.
37. Graff, R. A.; Swanson, T. M.; Strano, M. S. Synthesis of Nickel-Nitrilotriacetic Acid Coupled Single-Walled Carbon Nanotubes for Directed Self-Assembly with Polyhistidine-Tagged Proteins. *Chem. Mater.* **2008**, *20*, 1824–1829.
38. Lu, Y.; Goldsmith, B. R.; Kybert, N. J.; Johnson, A. T. C. DNA-Decorated Graphene Chemical Sensors. *Appl. Phys. Lett.* **2010**, *97*, 083107.

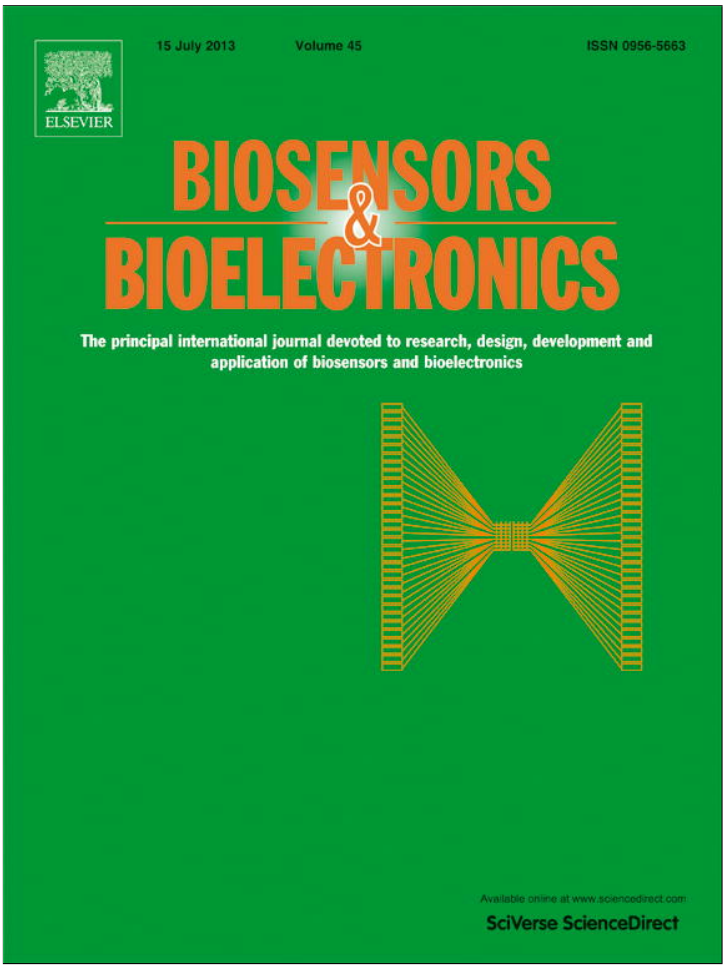

Biosensors and Bioelectronics 45 (2013) 163–167

Contents lists available at SciVerse ScienceDirect

Biosensors and Bioelectronics

journal homepage: www.elsevier.com/locate/bios

Short communication

Detecting Lyme disease using antibody-functionalized single-walled carbon nanotube transistors

Mitchell B. Lerner [a,1], Jennifer Dailey [a,1], Brett R. Goldsmith [a,2], Dustin Brisson [b], A.T. Charlie Johnson [a,*]

[a] Department of Physics and Astronomy, University of Pennsylvania, 209 South 33rd Street, Philadelphia, PA 19104, USA
[b] Department of Biology, University of Pennsylvania, 3740 Hamilton Walk, Philadelphia, PA 19104, USA

ARTICLE INFO

Article history:
Received 17 October 2012
Received in revised form
13 January 2013
Accepted 21 January 2013
Available online 4 February 2013

Keywords:
Carbon nanotubes
Lyme
FET

ABSTRACT

We examined the potential of antibody-functionalized single-walled carbon nanotube (SWNT) field-effect transistors (FETs) to use as a fast and accurate sensor for a Lyme disease antigen. Biosensors were fabricated on oxidized silicon wafers using chemical vapor deposition grown carbon nanotubes that were functionalized using diazonium salts. Attachment of *Borrelia burgdorferi* (Lyme) flagellar antibodies to the nanotubes was verified by atomic force microscopy and electronic measurements. A reproducible shift in the turn-off voltage of the semiconducting SWNT FETs was seen upon incubation with *B. burgdorferi* flagellar antigen, indicative of the nanotube FET being locally gated by the residues of flagellar protein bound to the antibody. This sensor effectively detected antigen in buffer at concentrations as low as 1 ng/ml, and the response varied strongly over a concentration range coinciding with levels of clinical interest. Generalizable binding chemistry gives this biosensing platform the potential to be expanded to monitor other relevant antigens, enabling a multiple vector sensor for Lyme disease. The speed and sensitivity of this biosensor make it an ideal candidate for development as a medical diagnostic test.

1. Introduction

Lyme disease is a tick-borne illness caused by the bacteria *Borrelia burgdorferi*, generating at least 30,000 new cases in the United States each year, although there are likely many more cases that go undetected or misdiagnosed due to generality of symptoms (Centers for Disease Control and Prevention, 2011). Of the patients diagnosed with Lyme disease, many are originally misdiagnosed due to the general symptoms of the disease (Williams et al., 1990), inconsistent disease presentation in patients (Aguerorosenfeld et al., 1993), and lack of sensitive testing available for early stages of the infection (Bakken et al., 1997). Late detection of Lyme disease can result in further complications including arthritis and permanent neurological disorders (Marques, 2008). Diagnosis of Lyme disease is severely hindered by the lack of reliable diagnostic tools despite its importance to treatment success (Murray and Shapiro, 2010; O'Connell, 2010). A reliable and rapid laboratory diagnostic tool is crucial for reducing the number of misdiagnosed patients and for investigating appropriate treatment protocols for chronic Lyme disease.

In recent years, great progress has been made in the field of carbon nanotube field effect transistor (CNT FET)-based biosensors (Allen et al., 2007). Benefits of nanotube-based sensors include the speed and reliability obtained from performing multiple assays in parallel (Chikkaveeraiah et al., 2009). Protein-functionalized nanotube-based FETs are of great research and clinical interest for several reasons. Their nanometer size is comparable to the size of many biomolecules of interest, suggesting a unique biocompatible platform (Harrison and Atala, 2007; Lerner et al., 2011; Sudibya et al., 2009). Additionally, since every atom of a carbon nanotube is located on its surface, in direct contact with the environment, they are a clear choice for direct environmental sensing. Commercially available assays for Lyme-specific antigens in urine and cerebrospinal fluid have a limit of detection of 12–15 ng/mL (Shah et al., 2004). We hypothesized that an antibody-functionalized SWNT FET immunosensor would be able to detect the small amount of Lyme antigen that is present in bodily fluids at very early stages of Borrelia infection (Harris and Stephens, 1995) since protein-functionalized nano-enabled sensors have demonstrated very low detection limits, on the order of fM (Duan et al., 2012; Lerner et al., 2012a). Direct detection of the antigen provides

* Corresponding author. Tel.: +1 2158989325
E-mail address: cjohnson@physics.upenn.edu (A.T. Charlie Johnson).
[1] These authors contributed equally to this work.
[2] Current address: SPAWAR Systems Center Pacific, 53560 Hull Street, San Diego, CA 92152, USA.

0956-5663/$ - see front matter © 2013 Elsevier B.V. All rights reserved.
http://dx.doi.org/10.1016/j.bios.2013.01.035

earlier test results because it eliminates the delay required for the immune system to produce sufficient quantities of antibodies to be detected via Western Blot or ELISA, which can improve patient prognosis (Ma et al., 1992). Here we demonstrate that antibody-functionalized SWNT FET devices are effective biosensors for rapidly detecting Lyme flagellar antigen at clinically relevant concentrations, as low as 1 ng/ml, with negligible response to negative-control proteins and to pure buffer solution.

2. Materials and methods

2.1. Device fabrication

Carbon nanotube transistors were fabricated using previously described methods (Goldsmith et al., 2011; Khamis et al., 2011). Briefly, a solution of iron (III) nitrate dissolved in isopropanol was spin coated onto a p^{2+} doped Si/SiO_2 wafer to give an iron catalyst layer. Single-walled carbon nanotubes were grown by catalytic chemical vapor deposition (CVD) with methane (2500 sccm) as the carbon source in a background of forming gas (600 sccm Ar, 320 sccm H_2) at 900 °C for 2 min. Following the growth, an optimized bilayer photolithography process using PMGI and Shipley 1813 (Khamis et al., 2011) was used to pattern source and drain electrodes with 2.5 μm channel length that were then metallized (3 nm Ti/40 nm Pd) using thermal evaporation. The doped silicon substrate served as a global backgate to complete the three terminal field-effect transistor geometry. Devices were individually characterized by sweeping the back gate voltage from -10 V to 10 V while holding the bias voltage fixed at 100 mV. Approximately 80 high quality semiconducting SWNT devices with ON/OFF ratios >1000 were selected to use in experiments.

2.2. Protein functionalization

Monoclonal Lyme antibodies specific for *B. Burgdorferi* flagellar antigen (p41) were obtained commercially (antibodies-online.com). Histidine-tagged Lyme antigen containing the p41 flagellar immunodominant region (also known as flagellin) was obtained from ProSpec. Antigen was diluted with Tris–HCl buffer (pH 7.5), aliquoted to several concentrations and stored at 4 °C. Antibodies were aliquoted at a concentration of 1 μg/ml in Tris–HCl buffer and stored at −20 °C.

Nanotube functionalization followed previously documented procedures (Goldsmith et al., 2011; Lerner et al., 2012a) adapted from (Strano et al., 2003) (see Fig. 1). Carbon nanotubes were functionalized using diazonium salts synthesized according to a published recipe (Saby et al., 1997). Samples were immersed in a solution of 4-carboxybenzene diazonium tetrafluoroborate at a concentration of 2.5 mg/1 mL deionized (DI) water for 1 h at 40 °C to create sp^3 hybridization sites ending in carboxylic acid groups, then rinsed for 1 min each in acetone, methanol, and deionized water baths. The carboxylic acid groups were then activated with EDC and stabilized with sulfo-NHS at concentrations of 6 mg and 16 mg per 15 mL MES buffer (pH 6.0) respectively for 15 min at room temperature, followed by a DI water rinse. A solution of antibodies at a concentration of 1 μg/mL was pipetted onto the nanotube devices in a humid environment to prevent the solution from evaporating, causing primary amines on the antibody to displace stabilized sulfo-NHS sites over a period of 1 h. The devices were washed thoroughly by rinsing in two DI water baths for 2 min each and dried with gentle (less than 20 psi) nitrogen flow in order to minimize the amount of salts and non-specifically bound proteins on the device.

Antibody-functionalized SWNT-FET devices were similarly exposed to droplets of antigen at a known concentration for 20 min in a humid environment to prevent the droplet from evaporating. Exposure to Lyme flagellar antigen occurred over a sufficiently long time for the proteins to diffuse to the sensor and establish equilibrium between bound and unbound species. This is known to be a critical consideration for detection of biomolecular analytes at pM or lower concentration (Squires et al., 2008). The devices were then washed in two DI water baths for 2 min each to remove non-specifically bound antigen and dried with gentle nitrogen flow. Each device was exposed to only one concentration of antigen in order to avoid contamination of samples, and each concentration of antigen was tested on 5–10 functionalized devices to ensure reproducibility of the results.

3. Results and discussion

In order to verify the validity of the attachment chemistry, Atomic Force Microscopy (AFM) data were gathered on an Asylum AFM in tapping mode followed by both antibody attachment (Fig. 2a) and subsequent exposure to flagellar antigen at a concentration of 400 ng/mL (Fig. 2b). Fig. 2a (Fig. 2b) is an AFM image showing small ball-like features that are associated with bound antibodies (antibody/antigen complexes), with a density ca. 3-5 attachments per micrometer. As is typically found in AFM analysis, the lateral dimension of the features (~50 nm in Fig. 2b) is larger than the molecular size, which is an artifact associated with the finite radius of the AFM tip. The *height* of the features is therefore compared with the expected size of the antibody and antibody/antigen complex. Statistical analysis of the feature heights in Fig. 2a shows that the antibodies are $2.78\ \text{nm} \pm 0.22\ \text{nm}$ in size, slightly smaller than expected for a complete IgG. This is likely due to the protein being slightly distorted during the tapping mode AFM in air, as we have reported previously (Johnson et al., 2009; Zhang et al., 2007). After exposure to flagellar antigen, the histogram of feature heights shows new peaks at 4.7 ± 0.6 nm and 6.5 ± 0.4 nm associated with larger antibody/antigen complexes. These are ascribed to binding of one and two antigen proteins, respectively, to a bound antibody, consistent with the fact that the IgG used in the experiments has two binding sites (Talwar and Srivastava, 2006). Each added antigen increases the feature height by ~1.8 nm. There also appears to be an additional minor peak at ~3 nm that represents unreacted antibodies; this peak accounts for ~20% of the total features measured. These data suggest that after exposure to antigen at 400 ng/mL, approximately 80% of the antibodies have bound to at least one antigen, in good agreement with the electronic response data presented in Fig. 3b.

We conducted a control experiment to establish that nanotubes and the nanotube/SiO_2 interface show very low affinity for non-specific binding of the Lyme antigen; details are provided in Supplementary material Fig. S1. When as-prepared nanotube devices were exposed to a high concentration (1 μg/mL) of Lyme antigen, there was minimal non-specific binding to the nanotubes or to the surrounding substrate. We also confirmed that exposure to the Lyme antigen at this concentration had negligible effect on the electronic characteristics of the device. These control experiments provide strong evidence that the biosensor responses described below reflect specific binding of the antigen.

Electronic measurements of the current as a function of the backgate voltage (I–V_g characteristics) for individual NT FET devices were taken following each chemical modification to monitor the effect of chemical functionalization and to confirm attachment of antibodies (Fig. 3a). Parameters of interest included I_{ON}, the ON state current of the device, and V_{TH}, the threshold voltage, where the line tangent to the I–V_g curve intersects the gate voltage axis. A 50–90% drop in I_{ON} as well as a 3–4 V decrease in

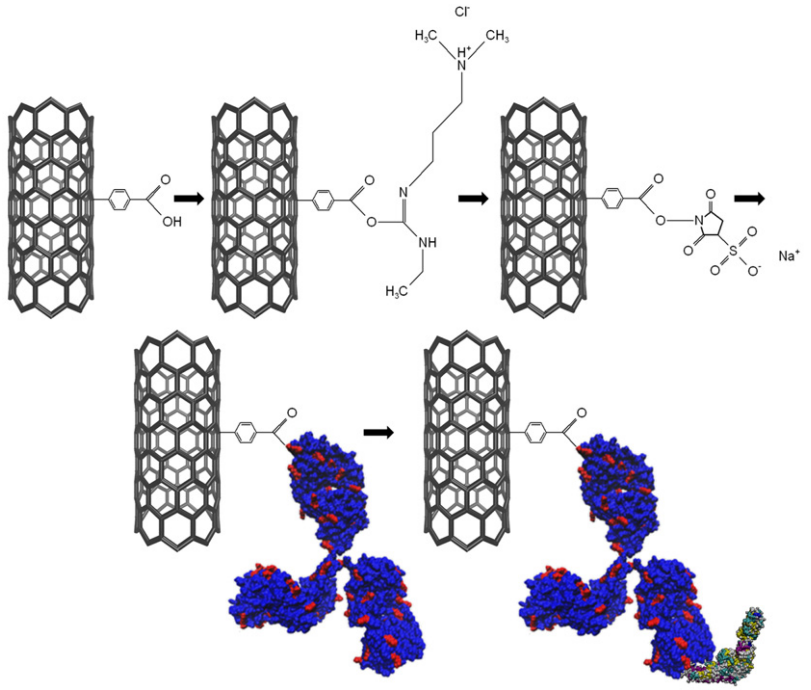

Fig. 1. Functionalization chemistry for Lyme antibody and binding of flagellar antigen. First, a pristine nanotube is treated with diazonium salts to create sp^3 hybridization sites ending in carboxylic acid moieties. The carboxylic acid is activated with EDC and stabilized with sulfo-NHS. The sulfo-NHS is displaced by the primary amine in a surface lysine residue (depicted in red) on the anti-p41 antibody. The flagellar antigen (depicted according to secondary structure in purple, cyan, and yellow) then binds to the epitope on the antibody during the exposure step. (For interpretation of the references to color in this figure legend, the reader is referred to the web version of this article.)

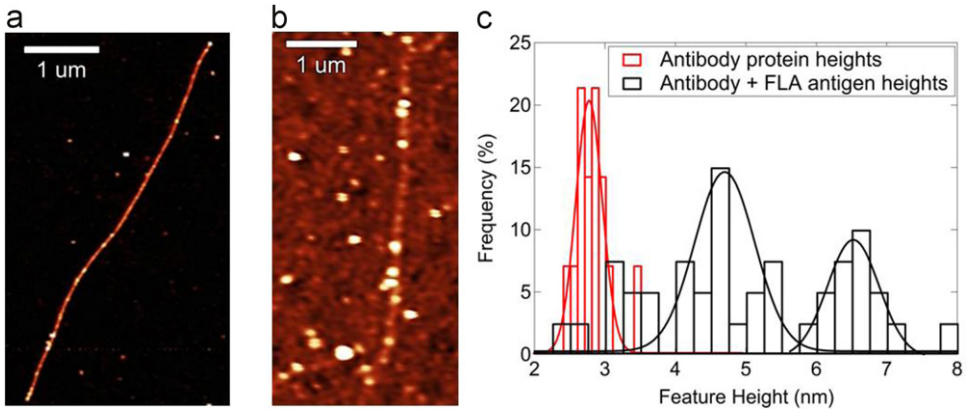

Fig. 2. (a) AFM image of anti-p41 antibody proteins attached to carbon nanotubes. *Z* scale is 6 nm, average protein feature is ~2.8 nm in size. (b) AFM image after incubation in a solution of FLA antigen at a concentration of 400 ng/mL shows antigen attached to bound antibodies on a nanotube. *Z* scale is 8 nm. (c) Histogram of feature heights following antibody attachment (red data) and exposure to antigen (black data). (For interpretation of the references to color in this figure legend, the reader is referred to the web version of this article.)

the threshold voltage resulted from diazonium oxidation, which is associated with the creation of sp^3 hybridization sites terminated with a carboxylic acid group. EDC/NHS treatment resulted in a slight decrease in the ON state current, while the change in the threshold voltage varied from sample to sample (e.g., V_{TH} shows a decrease in Fig. 3a and an increase in Fig S2 of the Supplemental material). The reason for this variation remains a subject for future research. Following antibody attachment, there was typically an increase in ON state current, suggesting that the attachment led to a decrease in carrier scattering. Upon antigen exposure, a shift in the threshold voltage toward more negative values was consistently observed. There was no statistically significant change in ON state current following antigen exposure.

There was a systematic dependence of the threshold voltage shift with varying antigen concentration in the range from 0.1 ng/ml to 3 μg/ml, with each concentration tested on 5–10 functionalized devices. The variation of the average measured shift in the threshold voltage as a function of antigen concentration is displayed in Fig. 3b. Error bars shown are the standard error of the mean. The sensor responses agree with a model based on the Hill–Langmuir equation for equilibrium protein binding (see Fig. 3b) (Hill, 1910; Lehninger et al., 2008):

$$\Delta V_{TH} = A\frac{(c/K_d)^n}{1+(c/K_d)^n} + Z$$

here c is the Lyme antigen concentration, A is the sensor response at saturation when all binding sites are occupied, Z is an overall offset to account for the response to pure buffer, K_d is the dissociation constant describing the concentration at which half

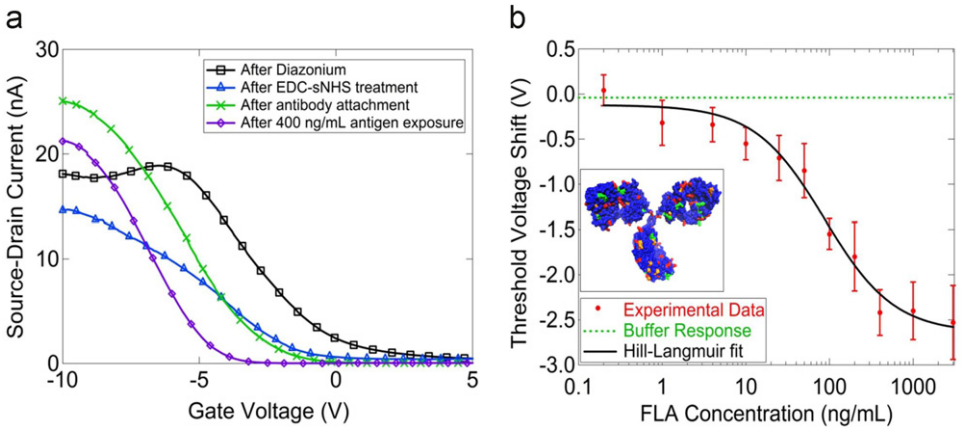

Fig. 3. (a) Current vs. gate voltage characteristics at subsequent stages of nanotube functionalization. The sensing response is 2.3 V decrease of the threshold voltage upon exposure to antigen (curve with green x to curve with purple diamond). (b) Threshold voltage shift as a function of antigen concentration can be fit with a model based on the Hill–Langmuir equation. These data indicate a limit of detection of ~1 ng/mL and non-cooperative antigen binding. Inset shows structure of anti-p41 Borrelia antibody with lysine (red), histidine (orange) and arginine (green) residues highlighted. Any of these basic residues could become protonated and generate a local gating effect if they come into closer contact with the nanotube upon antigen binding. (For interpretation of the references to color in this figure legend, the reader is referred to the web version of this article.)

of available binding sites are occupied, and n is the Hill coefficient describing cooperativity of binding.

The best fit to the data yielded a maximum response $A=-2.52\ \text{V}\pm0.32\ \text{V}$, offset parameter $Z=-0.12\ \text{V}\pm0.16\ \text{V}$, dissociation constant $K_d=87\ \text{ng/mL}\ \pm27\ \text{ng/mL}$, and $n=1.04\pm0.08$. The best fit value of the offset parameter $Z=-0.12\ \text{V}\ \pm0.16\ \text{V}$ was statistically indistinguishable from the experimentally measured responses of seven devices to pure buffer as a negative control ($\Delta V=0.11\ \text{V}\ \pm0.15\ \text{V}$). The value of $K_d=87\pm27\ \text{ng/mL}$ determined from the fit describes the concentration of antigen at which half the receptors are occupied; this regime coincides with antigen levels of diagnostic significance, 12–15 ng/mL (Shah et al., 2004). It is notable that the AFM image in Fig. 2b, taken after exposure to antigen at 400 ng/mL, shows occupation at ~80% of the attached antibody sites, in good agreement with the prediction of the Hill–Langmuir fit, that 95% of the active sites were occupied at this concentration. The slight discrepancy could be due to antibodies that were bound to the nanotube in such an orientation that their epitope is obstructed or otherwise non-functional. The Hill–Langmuir model combined with the AFM data suggested that the number of such antibodies unavailable for binding is no more than 20% of the total bound antibodies.

The best fit value of the cooperativity parameter, $n=1.04\pm0.08$, indicates independent binding of Lyme antigen to the anti-p41 in the context of the NT-FET biosensor. The data presented in Fig. 3b show that the measured responses from a collection of 5–10 devices could be used to differentiate between pure buffer solution ($\Delta V=0.11\ \text{V}\ \pm0.15\ \text{V}$) and buffer containing Lyme antigen at a concentration of 1 ng/mL ($\Delta V=-0.31\ \text{V}\ \pm0.24\ \text{V}$). Previous work suggests that this limit of detection may be lowered by as much as a factor of 1000 by replacing the complete IgG with its single chain variable fragment, thus allowing the binding event to occur closer to the nanotube where the electrostatic influence on transport in the NT transistor will be more pronounced (Lerner et al., 2012a). Although significant device-to-device variation was observed (as reflected in the error bars in Fig. 4), in this application the main concern is the detection of Lyme antigen at any level, rather than accurate measurement of its concentration. The results obtained in this experiment suggest that nanotube biosensors offer great promise for development into a useful diagnostic test.

The observed reduction in turnoff voltage is consistent with a gating effect due to the presence of positive charges in the local electrostatic environment of the carbon nanotube (Heller et al. 2008). The proposed mechanism responsible for introducing these positive local charges is a conformational change in the antibody protein upon binding the flagellar antigen, which results in the carbon nanotube being exposed to different amino acids on the antibody exterior. Charges in close proximity to carbon nanotubes have been shown to shift the transistor threshold voltage by local gating (Lerner et al., 2012b). Lysine, histidine, and arginine (highlighted in the inset of Fig. 3b) are common amino acids, a portion of which will be protonated when the pH is less than 7 and are thus candidates for locally gating the nanotube as observed. Experimental conditions may be as low as pH 5 due to deprotonation of silanol groups in a thin water layer that forms on the hydrophilic SiO_2 surface (Lerner et al., 2012b; O'Reilly et al., 2005). Even in the absence of a quantitative understanding of the device response, the results provide strong evidence that the methods used here enabled attachment of antibody proteins to a NT-FET while maintaining both the high quality electronic characteristics of the NT device and the chemical recognition functionality characteristic of the protein.

As a further control experiment, antibody-functionalized sensors were incubated in a solution of bovine serum albumin (BSA) at high concentration (1 μg/mL) to approximate the effect of non-specific proteins present in patient samples (human serum albumin is a large component of blood plasma proteins and represents a potential interfering agent; Peters, 1996). A sample I–V_g characteristic is presented in Supplementary material Fig. S2. The sensor response to BSA, averaged over eight devices, was a shift of $-0.13\ \text{V}\ \pm0.18\ \text{V}$, similar to the response produced by buffer alone. We thus concluded that the Lyme flagellar antibody-functionalized carbon nanotube transistors exhibited a high level of specificity for the flagellar protein target antigen.

4. Conclusions

We demonstrated that antibody-functionalized SWNT FET devices are effective biosensors for rapidly detecting Lyme disease antigen at diagnostically relevant concentrations. The sensor responses were rapid (minutes) and exhibited good reproducibility. We achieved detection of flagellar antigen protein at a concentration of 1 ng/ml with negligible response to control proteins and to pure buffer solution. The experiments showed an

antigen-specific, concentration-dependent sensor response over a wide range of concentrations (from 1 ng/mL to 3000 ng/mL) that was in excellent quantitative agreement with a model based on the Hill–Langmuir equation of equilibrium thermodynamics. Future work includes functionalizing samples with single chain variable fragments to increase sensitivity and the use of a sensor array based on multiple antibodies in order to capture several types of proteins indicative of Lyme disease for a multiplexed biosensor platform. The rapidity and ease of use of this sensor is superior to traditional immunoassays, suggesting its utility as a point-of-care diagnostic tool.

Acknowledgments

This research was supported by the Department of Defense US Army Medical Research and Materiel Command through Grants W81XWH-09-1-0205 and W81XWH-09-1-0206 (M.L., J.D. A.T.C.J.) and by the National Institutes of Health Grant R01AI076342 (D.B.). We acknowledge use of facilities associated with the Nano/Bio Interface Center, National Science Foundation NSEC DMR08-32802. J.D. acknowledges support of the REU program of the Laboratory for Research on the Structure of Matter (NSF REU Site Grant DMR-1062638) and of the Penn University Scholars program.

Appendix A. Supporting information

Supplementary data associated with this article can be found in the online version at http://dx.doi.org/10.1016/j.bios.2013.01.035.

References

Aguerorosenfeld, M.E., Nowakowski, J., Mckenna, D.F., Carbonaro, C.A., Wormser, G.P., 1993. Journal of Clinical Microbiology 31 (12), 3090–3095.
Allen, B.L., Kichambare, P.D., Star, A., 2007. Advanced Materials 19 (11), 1439–1451.
Bakken, L.L., Callister, S.M., Wand, P.J., Schell, R.F., 1997. Journal of Clinical Microbiology 35 (3), 537–543.
Centers for Disease Control and Prevention, 2011. N.C.f.E.a.Z.I.D.N., Division of Vector-Borne Diseases (DVBD), Lyme Disease: A Public Information Guide.
Chikkaveeraiah, B.V., Bhirde, A., Malhotra, R., Patel, V., Gutkind, J.S., Rusling, J.F., 2009. Analytical Chemistry 81 (21), 9129–9134.
Duan, X.X., Li, Y., Rajan, N.K., Routenberg, D.A., Modis, Y., Reed, M.A., 2012. Nature Nanotechnology 7 (6), 401–407.
Goldsmith, B.R., Mitala, J.J., Josue, J., Castro, A., Lerner, M.B., Bayburt, T.H., Khamis, S.M., Jones, R.A., Brand, J.G., Sligar, S.G., Luetje, C.W., Gelperin, A., Rhodes, P.A., Discher, B., Johnson, A.T.C., 2011. ACS Nano 5, 5408–5416.
Harris, N., Stephens, B.G., 1995. Journal of Spirochetal and Tick-borne Diseases 2, 37–41.
Harrison, B.S., Atala, A., 2007. Biomaterials 28 (2), 344–353.
Heller, I., Janssens, A.M., Mannik, J., Minot, E.D., Lemay, S.G., Dekker, C., 2008. Nano Letters 8 (2), 591–595.
Hill, A., 1910. Journal of Physiology 40, 4–7.
Johnson, R.R., Rego, B.L., Johnson, A.T.C., Klein, M.L., 2009. Journal of Physical Chemistry B 113, 11589–11593.
Khamis, S.M., Jones, R.A., Johnson, A.T.C., 2011. AIP Advances 1, 022106.
Lehninger, A.L., Nelson, D.L., Cox, M.M., 2008. Lehninger Principles of Biochemistry, 5th ed. W.H. Freeman, New York.
Lerner, M.B., D'Souza, J., Pazina, T., Dailey, J., Goldsmith, B.R., Robinson, M.K., Johnson, A.T.C., 2012a. ACS Nano 6 (6), 5143–5149.
Lerner, M.B., Goldsmith, B.R., McMillon, R., Dailey, J., Pillai, S., Singh, S.R., Johnson, A.T.C., 2011. AIP Advances 1, 042127.
Lerner, M.B., Resczenski, J.M., Amin, A., Johnson, R.R., Goldsmith, J.I., Johnson, A.T., 2012b. Journal of the American Chemical Society 134 (35), 14318–14321.
Ma, B., Christen, B., Leung, D., Vigo-Pelfrey, C., 1992. Journal of Clinical Microbiology 30 (2), 370–376.
Marques, A., 2008. Infectious Disease Clinics of North America 22 (2), 341–360 vii–viii.
Murray, T.S., Shapiro, E.D., 2010. Clinics in Laboratory Medicine 30 (1), 311–328.
O'Connell, S., 2010. Current Opinion in Infectious Diseases 23 3, 231–235.
O'Reilly, J.P., Butts, C.P., I'Anson, I.A., Shaw, A.M., 2005. Journal of the American Chemical Society 127 (6), 1632–1633.
Peters, T., 1996. All About Albumin: Biochemistry, Genetics, and Medical Applications. Academic Press, San Diego.
Saby, C., Ortiz, B., Champagne, G.Y., Belanger, D., 1997. Langmuir 13 (25), 6805–6813.
Shah, J., Harris, N., Bai, H., Remollo, G., 2004. Assay for Detection of Antigen in Bodily Fluid. In: Office, U.S.P.A.T. (Ed.). IGeneX, Inc., Palo Alto, CA, United States of America.
Squires, T.M., Messinger, R.J., Manalis, S.R., 2008. Nature Biotechnology 26 (4), 417–426.
Strano, M.S., Dyke, C.A., Usrey, M.L., Barone, P.W., Allen, M.J., Shan, H.W., Kittrell, C., Hauge, R.H., Tour, J.M., Smalley, R.E., 2003. Science 301 (5639), 1519–1522.
Sudibya, H.G., Ma, J.M., Dong, X.C., Ng, S., Li, L.J., Liu, X.W., Chen, P., 2009. Angewandte Chemie International Edition 48 (15), 2723–2726.
Talwar, G.P., Srivastava, L.M., 2006. Textbook of Biochemistry and Human Biology, 3rd ed. Prentice-Hall of India Private Limited, New Delhi, India.
Williams, C.L., Strobino, B., Lee, A., Curran, A.S., Benach, J.L., Inamdar, S., Cristofaro, R., 1990. The Pediatric Infectious Disease Journal 9 (1), 10–14.
Zhang, Y.B., Kanungo, M., Ho, A.J., Freimuth, P., van der Lelie, D., Chen, M., Khamis, S.M., Datta, S.S., Johnson, A.T.C., Misewich, J.A., Wong, S.S., 2007. Nano Letters 7 (10), 3086–3091.

JACS
JOURNAL OF THE AMERICAN CHEMICAL SOCIETY

Communication

pubs.acs.org/JACS

Toward Quantifying the Electrostatic Transduction Mechanism in Carbon Nanotube Molecular Sensors

Mitchell B. Lerner,[†] James M. Resczenski,[†] Akshay Amin,[†] Robert R. Johnson,[†] Jonas I. Goldsmith,*[,‡] and A. T. Charlie Johnson*[,†]

[†]Department of Physics and Astronomy, University of Pennsylvania, 209 South 33rd Street, Philadelphia, Pennsylvania 19104, United States

[‡]Department of Chemistry, Bryn Mawr College, 101 North Merion Avenue, Bryn Mawr, Pennsylvania 19010, United States

Supporting Information

ABSTRACT: Despite the great promise of carbon nanotube field-effect transistors (CNT FETs) for applications in chemical and biochemical detection, a quantitative understanding of sensor responses is lacking. To explore the role of electrostatics in sensor transduction, experiments were conducted with a set of highly similar compounds designed to adsorb onto the CNT FET via a pyrene linker group and take on a set of known charge states under ambient conditions. Acidic and basic species were observed to induce threshold voltage shifts of opposite sign, consistent with gating of the CNT FET by local charges due to protonation or deprotonation of the pyrene compounds by interfacial water. The magnitude of the gate voltage shift was controlled by the distance between the charged group and the CNT. Additionally, functionalization with an uncharged pyrene compound showed a threshold shift ascribed to its molecular dipole moment. This work illustrates a method for producing CNT FETs with controlled values of the turnoff gate voltage, and more generally, these results will inform the development of quantitative models for the response of CNT FET chemical and biochemical sensors.

Single-walled carbon nanotubes (CNTs) have shown great promise for use as chemical sensors. Various surface modifications have been used to create nanoenabled, all-electronic vapor sensors,[1,2] electrochemical cells for small-molecule detection,[3,4] and fast electronics-based protein detection.[5−7] However, the detection mechanisms for these devices remain incompletely understood. Pyrene-containing compounds have been shown to adsorb specifically onto CNTs through $\pi-\pi$ stacking, and this adsorption process has been measured in situ by electrochemical methods.[8] This makes the use of pyrene compounds ideal for exploring transduction mechanisms, since they provide a method to position known chemical groups precisely with respect to the nanotube sidewall.

Here, single-walled CNT field-effect transistors (CNT FETs) were functionalized with the pyrene compounds shown in Figure 1. The turnoff threshold voltage (i.e., the back-gate voltage required to suppress conduction in the FET) was measured for the functionalized devices and found to shift as the acid−base properties of the pyrene molecules were varied.

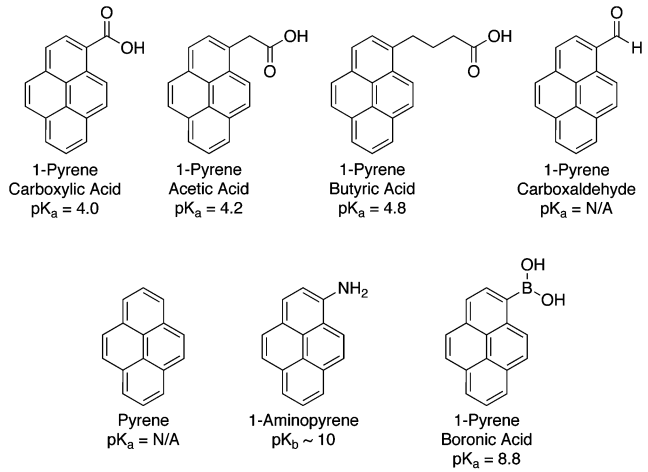

Figure 1. Pyrene compounds utilized in this work. Quoted values of pK_a and pK_b are from refs 10−14. Where actual pK_a values were not avaliable, values were estimated by comparison to those of related compounds: naphthylacetic acid for 1-pyreneacetic acid, naphthylamine for 1-aminopyrene, and phenylboronic acid for 1-pyreneboronic acid.

This shift was attributed to chemical (electrostatic) gating[9] of the CNT FET by protonated/deprotonated groups on the pyrene molecules. The size of the threshold voltage shift was controlled by the distance between the charged group and the CNT sidewall, leading to insights about the nature of the electrostatic interaction. Interestingly, a neutral compound induced a threshold gate voltage shift that was attributed to its intrinsic dipole moment. The magnitude of the observed threshold voltage shifts were in qualitative agreement with estimates of the charge densities associated with the adsorbed pyrene molecules. The work illustrates a practical functionalization scheme and shows how one could tailor the threshold voltage of CNT FETs by judicious choice of a compound. These results also help in building a quantitative understanding of electrostatic detection mechanisms in CNT FET molecular sensors.

Pyrene, 1-pyrenecarboxylic acid, 1-aminopyrene, and 1-pyreneacetic acid were purchased from Sigma-Aldrich; 1-

Received: June 29, 2012
Published: August 15, 2012

dx.doi.org/10.1021/ja306363v | J. Am. Chem. Soc. 2012, 134, 14318−14321

pyrenebutyric acid and 1-pyrenecarboxaldehyde from Alfa Aesar; and 1-pyrene boronic acid from TCI. The solvent used for all solutions was high-purity acetonitrile (Honeywell Burdick & Jackson, 99.9% pesticide residue grade). All chemicals were used as received. To make solutions of various pyrenes, concentrated stock solutions (ca. 1 mM) were prepared by dissolving a small amount (ca. 5 mg) of each pyrene in 20.0 mL of CH_3CN. Several minutes of mixing using an ultrasonic bath were required to effect complete dissolution. The stock solutions were diluted to yield 5 μM pyrene solutions in CH_3CN.

CNT FETs were fabricated as described previously.[15] Briefly, CNTs were grown on Si/SiO_2 substrates by chemical vapor deposition at 900 °C using iron nanoparticles as the catalyst. Source–drain electrodes were patterned by photolithography and metallized with 3 nm Ti/40 nm Pd deposited in a thermal evaporator. After liftoff, devices were annealed in ambient atmosphere at 250 °C for 1 h to remove excess photoresist residue.[15] The underlying doped silicon substrate served as a global back gate in a three-terminal FET geometry.

The CNT FETs were characterized by measuring the source–drain current (I) as a function of gate voltage (V_G) at a bias voltage of 100 mV. Two criteria were used to select devices consisting of single semiconducting nanotubes for subsequent experiments: (1) devices dominated by hole conduction, with an ON/OFF ratio exceeding 100, and (2) device resistance in the range 100 kΩ to 2 MΩ. CNT FETs were functionalized by incubation in a solution of one of the pyrene compounds (5 μM in CH_3CN) for 2 h, rinsed for 5 min each in CH_3CN, isopropanol, and deionized water, and then blown dry with clean nitrogen. Previous work on pyrene adsorption onto glassy carbon[16] suggested that this process would lead to complete saturation of available pyrene binding sites; lower values of the pyrene solution concentration or functionalization time might in the future be used to fine-tune the density of adsorbed pyrene molecules. Samples were baked on a hot plate at 120 °C for 2 h to remove remaining solvents. Between 15 and 20 devices were functionalized by this process for each pyrene compound shown in Figure 1.

The effectiveness of the functionalization procedure was confirmed via atomic force microscopy (AFM) and X-ray photoelectron spectroscopy (XPS). AFM images (Figure 2a,b) showed that the height of the CNTs increased by ca. 0.8 nm after functionalization, consistent with what would be expected from the interlayer spacing of a graphitic system[17] such as a CNT and an absorbed pyrene compound. The XPS spectrum of a device functionalized with 1-aminopyrene (Figure 2c) showed a peak at 287.0 eV indicative of the C–N bond of 1-aminopyrene bound on the CNT as well as peaks at 284.8 and 289.0 eV characteristic of C–C and C–O bonding, respectively. Consistent with expectations, samples of untreated CNTs, acetonitrile-treated CNTs, and bare SiO_2 treated with 1-aminopyrene did not show the C–N peak (Figure 2c).

Electrical measurements were performed after functionalization, and changes in the I–V_G curve were noted, especially changes in the transistor threshold voltage (ΔV_T) (Figure 3). Functionalization with pyrene compounds had little effect on the CNT FET ON state resistance and hole carrier mobility, consistent with the intuition that noncovalent functionalization should not introduce significant carrier scattering. As discussed below, the results can be explained quantitatively by a picture in which the value of ΔV_T is determined by electrostatic chemical gating of the CNT FET by the adsorbed pyrene molecules.

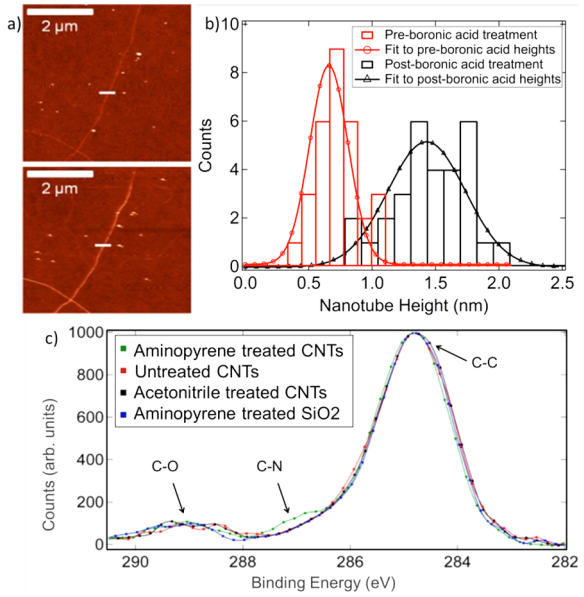

Figure 2. (a) AFM images of a CNT (top) before and (bottom) after treatment with 5 μM 1-pyreneboronic acid. The Z scale is 6 nm. (b) Histograms based on 30 line scans at the same positions before and after treatment with 1-pyreneboronic acid. The evident ca. 0.8 nm increase in height is attributed to the presence of adsorbed pyrene molecules. (c) XPS spectra under several sets of experimental conditions. The peak at 287.0 eV indicates the presence of C–N bonds in the sample of CNTs treated with 1-aminopyrene.

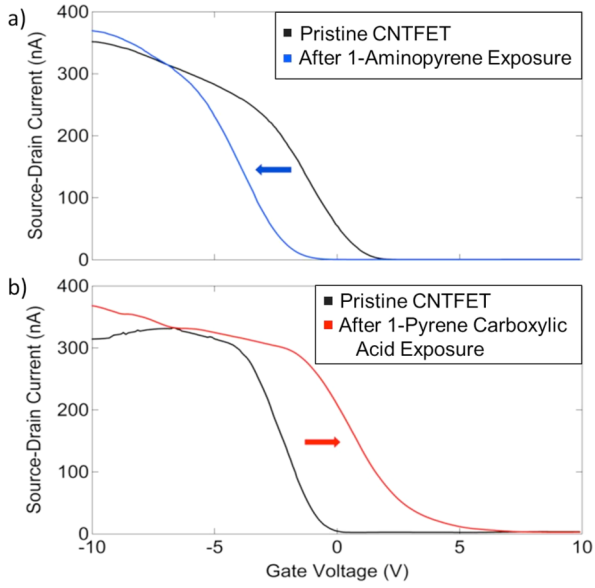

Figure 3. (a) I–V_G plot for a CNT FET functionalized with 1-aminopyrene, showing a shift toward negative V_G. (b) Similar data for a device functionalized with 1-pyrenecarboxylic acid, showing a shift toward positive V_G.

Since a thin surface layer of water exists on CNT FET devices on SiO_2 under ambient atmosphere, its effect on the charge state of the adsorbed pyrene molecules must be considered. Recent work has demonstrated that silanol groups on the surface of SiO_2 cause near-surface water to be considerably more acidic than bulk water (by ca. 2 pH units).[18] Pyrene-functionalized CNT FET devices on SiO_2 are

dx.doi.org/10.1021/ja306363v | J. Am. Chem. Soc. 2012, 134, 14318–14321

thus best understood as operating in a slightly acidic aqueous medium (ca. pH 5).

The observed values of ΔV_T are summarized in Figure 4; they were reproducible for each of the pyrene compounds

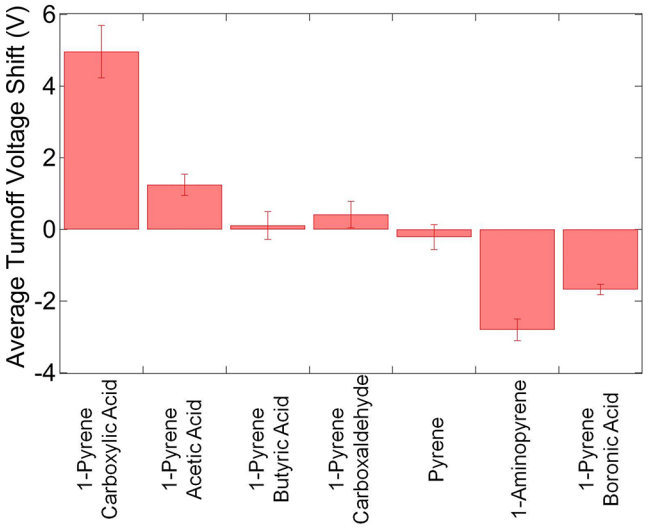

Figure 4. Average threshold voltage shift, ΔV_T, caused by exposure to pyrene compounds. Each value is the average of results from 15−20 devices; error bars are standard errors of the mean.

tested. Adsorption of pyrene on the CNT FET led to a statistically insignificant shift in V_T (−0.2 ± 0.4 V); a similarly small shift was observed for 1-pyrenecarboxaldehyde (0.4 ± 0.4 V). These findings are consistent with the expectation that both compounds are in a neutral charge state under the experimental conditions and should have little or no effect on the $I(V_G)$ characteristic of the FET. The sign of ΔV_T was positive for each of the three pyrenecarboxylic acids tested and negative for 1-aminopyrene. These observations are consistent with the equilibrium constants listed in Figure 1. As the pK_a values for all of the pyrenecarboxylic acids are less than 5, most of the carboxylic acid functional groups should be deprotonated and negatively charged. The $I(V_G)$ characteristic is thus expected to shift to a more positive gate voltage ($\Delta V_T > 0$). Similarly, for 1-aminopyrene at pH 5, a fraction (ca. 10−15%) of the amine groups should be protonated, leading to a negative value of ΔV_T. The case of 1-pyreneboronic acid is unusual and will be discussed below.

Interpretation of the data is informed by a calculation of N, the density of singly charged species adsorbed on the CNT sidewall (presumed to be pyrene molecules) required to produce an observed value of ΔV_T: $N = |C\Delta V_T/e|$, where C is the CNT capacitance per unit length and e is the proton charge. The capacitance per unit length of a CNT FET in the backgate geometry is $C = 2\pi\varepsilon\varepsilon_0/\ln(2h/r)$, where r is the CNT radius and h and ε are the thickness and dielectric constant of the insulator between the CNT and the back gate, respectively.[19] For the device geometry used here, this equates to $N \approx 200$ charged molecules μm^{-1} V^{-1}.

The observed threshold voltage shift for 1-pyrenecarboxylic acid, ΔV_T = +5.0 ± 0.7 V, would require $N \approx 1000$ negative charges/μm. By geometrical stacking arguments, full monolayer coverage of pyrenes comprises ca. 9000 molecules/μm. A lower bound of 3000 molecules/μm is suggested by recent measurements of the coverage for pyrenes coupled to transition-metal complexes that are significantly larger than the functional groups of the molecules used here.[8] For this discussion, a density of 6000/μm is assumed. In a water layer at pH 5, roughly 90% of the carboxylic acid functional groups (i.e., ca. 5000 μm^{-1}) are deprotonated. Since the calculation suggests that 1000 deprotonated groups/μm are needed to produce the observed threshold voltage shift, we conclude that the gating effect of the charged groups is reduced by a factor of ca. 5 due to screening. For 1-aminopyrene (ΔV_T = −2.8 ± 0.3 V), a similar density of adsorbed molecules would be expected, but only 15% of the molecules should be charged (i.e., 4.5 times fewer than for pyrenecarboxylic acid). This argument leads to a predicted threshold voltage shift of −1.1 V, a factor of ca. 2.5 less than what was observed. This could be explained by a difference in the screening effect in the two cases or an environment with pH lower than 5, which would result in a smaller fraction of deprotonated carboxylic acid groups and a larger fraction of protonated amino groups. With these caveats, this framework provides a satisfactory semiquantitative explanation of the observations.

It was also observed that varying the compound containing the carboxyl group (carboxylic acid to acetic acid to butyric acid) led to a systematic reduction in the measured value of ΔV_T (+5.0 ± 0.7 to +1.2 ± 0.3 to +0.1 ± 0.4 V, respectively). This progression is attributed primarily to successively larger displacements of the charged carboxyl group away from the CNT sidewall; a secondary contributing factor is the reduced probability of deprotonation of the carboxyl group because of the differing pK_a values of the compounds. Molecular dynamics (MD) simulations (see the Supporting Information for details) indicated that the distance between the CNT sidewall and the carboxyl group of 1-pyrenecarboxylic acid is 0.34 nm, approximately equal to the interlayer spacing for graphene. This is interpreted as the effective electrostatic radius of the CNT and the pyrene molecule, each extending 0.17 nm into the adjoining space, so the relevant distance for electrostatic influence (i.e., the distance between the centers of the electron charge distributions) is 0.17 nm. The carboxyl group in 1-pyreneacetic acid is 0.12 nm farther from the CNT than in the case of 1-pyrenecarboxylic acid. If Coulomb interactions between the carboxyl group and the CNT are assumed and the reduction in protonation caused by the change of 0.2 units in pK_a is taken into account, this increased distance corresponds to a reduction in the interaction strength by a factor of 3.2, which can be compared with the observed reduction in ΔV_T by a factor of 4.1 ± 1.3. MD simulations indicated that the carboxyl group on 1-pyrenebutyric acid is 0.18 nm farther away than that of pyrenecarboxylic acid. This distance change coupled with the change in pK_a corresponds to a reduction by a factor of 4.3 and a predicted threshold shift of roughly 0.7 V. The measured shift for 1-pyrenebutyric acid is smaller (+0.1 ± 0.4 V), possibly because of more effective screening by water molecules, which can more readily penetrate between the carboxylic acid group and the nanotube surface for this molecule.

In contrast to other acids tested, functionalization with 1-pyreneboronic acid led to a negative value of ΔV_T (−1.7 ± 0.1 V); that is, the *sign* of the threshold voltage shift was characteristic of a base rather than an acid. To explain this, two facts are noted: (1) 1-pyreneboronic acid is a weak acid (pK_a = 8.8), so at pH 5, virtually all of the boronic acid molecules would be expected to be charge-neutral, and (2) the B−O bonds in boronic acids are highly polar, with the boron

dx.doi.org/10.1021/ja306363v | J. Am. Chem. Soc. 2012, 134, 14318−14321

(oxygen) atoms bearing a partial positive (negative) charge; thus, 1-pyreneboronic acid acts as an adsorbed dipole. Quantum-chemical simulations indicated a molecular dipole moment of ca. 2.6 D nearly coplanar with pyrene group. If a random orientation of the pyrenes adsorbed onto the CNT is assumed, on average the dipole will be oriented with the positively charged boron atom located closer to the CNT sidewall than the negatively charged oxygen by a distance of ca. 0.05 Å. On the basis of these considerations, it would be expected that the threshold voltage shift would be *negative* and approximately one-third that observed for the 1-aminopyrene case ($\Delta V_T = -2.8 \pm 0.3$ V). The observed value of the threshold voltage shift, $\Delta V_T = -1.7 \pm 0.1$ V, is thus attributed to the electrostatic effect of this dipole. The near-zero values of ΔV_T observed for pyrene and 1-pyrenecarboxaldehyde are consistent with this explanation, since neither of those species contains a bond as polarized as the B−O bonds in 1-pyreneboronic acid.

To summarize, we have demonstrated that pyrene compounds, which specifically absorb onto CNT FETs via a $\pi-\pi$ stacking interaction, can modify the transistor $I(V_G)$ characteristic through an electrostatic gating process. Acidic or basic functional groups interact with the interfacial water present on the CNT FET and become charged. These charged species anchored to the CNT gate the device, modifying the nanotube surface potential through electrostatic interactions. The change in surface potential results in a positive (negative) shift of the turnoff threshold voltage for negatively (positively) charged functional groups. Water-mediated local gating is thus a primary mechanism behind the responses of CNT FET molecular sensors. The magnitude of the threshold voltage shift was found to depend sensitively on the distance between the charged group and the CNT sidewall, behavior that can be understood qualitatively using an electrostatic model. The behavior of CNT FETs functionalized with uncharged 1-pyreneboronic acid is attributed to the effect of the molecular dipole moment, suggesting an explanation for reports in the literature where exposure to neutral molecules was found to elicit a distinct response from CNT FET sensors.[20,21]

Future work will involve experiments in buffer solution to modify the local pH at the SiO_2−water interface. This should modulate the degree of protonation for a given species and lead to threshold voltage shifts. The data presented here and obtained through the further investigations will inform the development of MD-based simulations that go beyond existing structural studies[22−24] to calculate the response of CNT FET chemical sensors due to electrostatic interactions.

■ ASSOCIATED CONTENT

Ⓢ Supporting Information

CNT FET schematic and details of the MD simulations. This material is available free of charge via the Internet at http://pubs.acs.org.

■ AUTHOR INFORMATION

Corresponding Author

jigoldsmit@brynmawr.edu; cjohnson@physics.upenn.edu

Notes

The authors declare no competing financial interest.

■ ACKNOWLEDGMENTS

This research was supported by the Department of Defense U.S. Army Medical Research and Materiel Command through Grant W81XWH-09-1-0206 and by the Nano/Bio Interface Center through NSF NSEC Grant DMR08-32802. J.M.R. was supported by the SUNFEST REU Program (NSF EEC-1062672). A.A. was supported by the Penn Undergraduate Research Mentoring Program. J.I.G. acknowledges support by a Faculty Startup Award from the Camille and Henry Dreyfus Foundation. This work made use of the XPS/Auger system at the Centralized Research Facilities at Drexel University. The acquisition of the XPS/Auger system was made possible through support from the NSF under Award CBET-0959361.

■ REFERENCES

(1) Goldsmith, B. R.; Mitala, J. J.; Josue, J.; Castro, A.; Lerner, M. B.; Bayburt, T. H.; Khamis, S. M.; Jones, R. A.; Brand, J. G.; Sligar, S. G.; Luetje, C. W.; Gelperin, A.; Rhodes, P. A.; Discher, B. M.; Johnson, A. T. C. *ACS Nano* **2011**, *5*, 5408.

(2) Pengfei, Q. F.; Vermesh, O.; Grecu, M.; Javey, A.; Wang, O.; Dai, H. J.; Peng, S.; Cho, K. J. *Nano Lett.* **2003**, *3*, 347.

(3) Wang, J.; Musameh, M. *Anal. Chem.* **2003**, *75*, 2075.

(4) Lin, Y. H.; Lu, F.; Tu, Y.; Ren, Z. F. *Nano Lett.* **2004**, *4*, 191.

(5) Chen, R. J.; Choi, H. C.; Bangsaruntip, S.; Yenilmez, E.; Tang, X. W.; Wang, Q.; Chang, Y. L.; Dai, H. J. *J. Am. Chem. Soc.* **2004**, *126*, 1563.

(6) Star, A.; Gabriel, J. C. P.; Bradley, K.; Gruner, G. *Nano Lett.* **2003**, *3*, 459.

(7) Lerner, M. B.; Pazina, T.; Robinson, M. K.; Johnson, A. T. C. *ACS Nano* **2012**, *6*, 5143.

(8) McQueen, E. W.; Goldsmith, J. I. *J. Am. Chem. Soc.* **2009**, *131*, 17554.

(9) Heller, I.; Janssens, A. M.; Mannik, J.; Minot, E. D.; Lemay, S. G.; Dekker, C. *Nano Lett.* **2008**, *8*, 591.

(10) Zelent, B.; Vanderkooi, J. M.; Coleman, R. G.; Gryczynski, I.; Gryczynski, Z. *Biophys. J.* **2006**, *91*, 3864.

(11) Sato, M.; Kaieda, T.; Ohmukai, K.; Kawazumi, H.; Harata, A.; Ogawa, T. *J. Phys. Chem. B* **2000**, *104*, 9873.

(12) Dippy, J. F. J.; Hughes, S. R. C.; Laxton, J. W. *J. Chem. Soc.* **1954**, 4102.

(13) *CRC Handbook of Chemistry and Physics*, 73rd ed.; CRC Press: Boca Raton, FL, 1992.

(14) Hall, D. G. *Boronic Acids: Preparation and Applications in Organic Synthesis, Medicine and Materials*; 2nd completely rev. ed.; Wiley-VCH: Weinheim, Germany, 2011.

(15) Khamis, S. M.; Jones, R. A.; Johnson, A. T. C. *AIP Adv.* **2011**, *1*, No. 022106.

(16) Smith, H. L.; Usala, R. L.; McQueen, E. W.; Goldsmith, J. I. *Langmuir* **2010**, *26*, 3342.

(17) Bernal, J. D. *Proc. R. Soc. London, Ser. A* **1924**, *106*, 749.

(18) O'Reilly, J. P.; Butts, C. P.; I'Anson, I. A.; Shaw, A. M. *J. Am. Chem. Soc.* **2005**, *127*, 1632.

(19) Martel, R.; Schmidt, T.; Shea, H. R.; Hertel, T.; Avouris, P. *Appl. Phys. Lett.* **1998**, *73*, 2447.

(20) Staii, C.; Chen, M.; Gelperin, A.; Johnson, A. T. *Nano Lett.* **2005**, *5*, 1774.

(21) Kauffman, D. R.; Star, A. *Angew. Chem., Int. Ed.* **2008**, *47*, 6550.

(22) Johnson, R. R.; Johnson, A. T. C.; Klein, M. L. *Nano Lett.* **2008**, *8*, 69.

(23) Johnson, R. R.; Kohlmeyer, A.; Johnson, A. T. C.; Klein, M. L. *Nano Lett.* **2009**, *9*, 537.

(24) Johnson, R. R.; Rego, B. L.; Johnson, A. T. C.; Klein, M. L. *J. Phys. Chem. B* **2009**, *113*, 11589.